Cell Reports
Medicine

Article

Single-cell transcriptomic landscape reveals tumor specific innate lymphoid cells associated with colorectal cancer progression

Graphical abstract

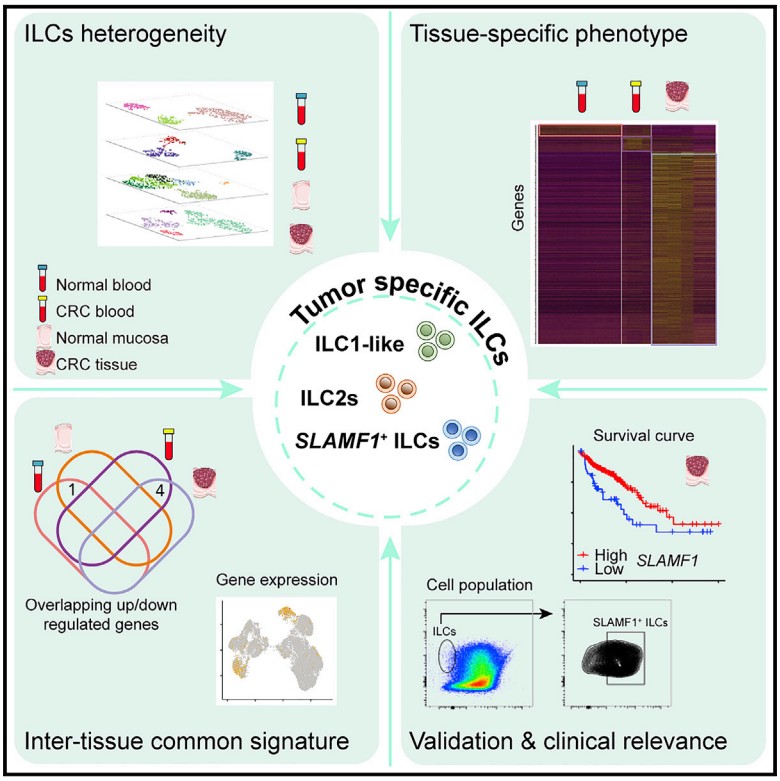

Highlights

- Healthy gut contains ILC1s, ILC3s, and ILC3/NKs, but no ILC2s
- Blood and tumor ILCs from CRC patients have unique transcriptomic features
- Tumor tissue from CRC patients contains a tumor specific ILC1-like subset and ILC2s
- SLAMF1 is identified as an anti-tumor biomarker in CRC

Authors

Jingjing Qi, Adeline Crinier, Bertrand Escalière, ..., Emilie Narni-Mancinelli, Eric Vivier, Bing Su

Correspondence

lshen@shsmu.edu.cn (L.S.), narni@ciml.univ-mrs.fr (E.N.-M.), vivier@ciml.univ-mrs.fr (E.V.), bingsu@sjtu.edu.cn (B.S.)

In brief

The roles and contribution of ILCs to cancer remain poorly defined. Through scRNA-seq profiling the landscape of ILCs from blood, normal mucosa, and tumor tissues from CRC patients, Qi et al. reveal the presence of tumor specific ILC subsets and an anti-tumor biomarker, SLAMF1, in CRC patients.

Qi et al., 2021, Cell Reports Medicine 2, 100353
August 17, 2021
https://doi.org/10.1016/j.xcrm.2021.100353

CellPress

Cell Reports Medicine

CellPress
OPEN ACCESS

Article

Single-cell transcriptomic landscape reveals tumor specific innate lymphoid cells associated with colorectal cancer progression

Jingjing Qi,[1,2,8] Adeline Crinier,[3,8] Bertrand Escalière,[3] Youqiong Ye,[1,2] Zhengting Wang,[4] Tianyu Zhang,[4] Luciana Batista,[5] Hongzhi Liu,[1,2] Liwen Hong,[4] Ningbo Wu,[1] Mingnan Zhang,[1] Lei Chen,[1] Yingbin Liu,[7] Lei Shen,[1,*] Emilie Narni-Mancinelli,[3,*] Eric Vivier,[3,5,6,*] and Bing Su[1,2,9,*]

[1]Shanghai Institute of Immunology, Department of Immunology and Microbiology, and the Ministry of Education Key Laboratory of Cell Death and Differentiation, Shanghai Jiao Tong University School of Medicine, Shanghai 200025, China
[2]Shanghai Jiao Tong University School of Medicine-Yale Institute for Immune Metabolism, Shanghai Jiao Tong University School of Medicine, Shanghai 200025, China
[3]Aix-Marseille Université, CNRS, INSERM, Centre d'Immunologie de Marseille-Luminy, 13009 Marseille, France
[4]Department of Gastroenterology, Ruijin Hospital, Shanghai Jiao Tong University School of Medicine, Shanghai 200025, China
[5]Innate Pharma Research Laboratories, Innate Pharma, 13009 Marseille, France
[6]Immunology, Marseille Immunopole, Hôpital de la Timone, Assistance Publique des Hôpitaux de 13005 Marseille, France
[7]Department of General Surgery, Xinhua Hospital Affiliated to Shanghai Jiao Tong University School of Medicine, Shanghai 200092, China
[8]These authors contributed equally
[9]Lead contact
*Correspondence: lshen@shsmu.edu.cn (L.S.), narni@ciml.univ-mrs.fr (E.N.-M.), vivier@ciml.univ-mrs.fr (E.V.), bingsu@sjtu.edu.cn (B.S.)
https://doi.org/10.1016/j.xcrm.2021.100353

SUMMARY

Innate lymphoid cells (ILCs) are tissue-resident lymphocytes differing from conventional T lymphocytes in having no antigen-specific receptors. ILCs include natural killer (NK) cells, helper-like ILC1s, ILC2s, and ILC3s, and lymphoid tissue-inducer (LTi) cells. Tumor ILCs are frequently found in various cancers, but their roles in cancer immunity and immunotherapy remain largely unclear. We report here the single-cell characterization of blood and gut helper-like ILC subsets in healthy conditions and in colorectal cancer (CRC). The healthy gut contains ILC1s, ILC3s, and ILC3/NKs, but no ILC2s. Additional tumor-specific ILC1-like and ILC2 subsets were identified in CRC patients. Signaling lymphocytic activation molecule family member 1 (SLAMF1) was found to be selectively expressed on tumor-specific ILCs, and higher levels of SLAMF1$^+$ ILCs were observed in the blood of CRC patients. The SLAMF1-high group of CRC patients had a significantly higher survival rate than the SLAMF1-low group, suggesting that SLAMF1 is an anti-tumor biomarker in CRC.

INTRODUCTION

T cell-based immunotherapy has been very successful clinically for the treatment of malignant tumors, but only in a small proportion of patients.[1–6] Treatments targeting other immune components are required to increase the proportion of patients benefiting from immunotherapy. Innate lymphoid cells (ILCs) are tissue-resident innate antigen-independent lymphocytes that regulate immunity to pathogens and commensal organisms for tissue homeostasis.[7,8] ILCs form a heterogeneous population of cells that are currently classified into five major groups, natural killer (NK) cells, helper-like ILC1s, ILC2s, and ILC3s, and lymphoid tissue-inducer (LTi) cells, on the basis of their cytokine production and transcription factor expression profiles.[8] ILCs are involved in immune functions, including pathogen responses, inflammation, tissue development, remodeling, repair, and homeostasis.

Given the large amounts and nature of the cytokines they produce, ILC subsets are likely to be involved in cancer immunity but may also contribute to tumor-associated inflammation. NK cells are known to play a role in cancer, through their tumor-suppressive properties, and are efficient at controlling metastasis.[9] The role of helper-like ILCs in the context of tumorigenesis and cancer immunity is less clear and appears to depend on the tumor microenvironment. ILC1s produce large amounts of proinflammatory cytokines, such as IFN-γ and TNF-α, which favor tumorigenesis.[10] However, IFN-γ can also limit tumor growth in certain tumor microenvironments.[11,12] ILC2s have been shown to be mostly detrimental in various tumor settings. Indeed, large numbers of ILC2s are present in the peripheral blood of patients with gastric cancer[13] and acute promyelocytic leukemia.[14] ILC2-derived IL-13 stimulates the immunosuppressive activity of myeloid-derived suppressor cells in acute promyelocytic leukemia[14] and in human bladder cancer and murine prostate tumors.[15] However, ILC2-derived IL-5 may help suppress primary and metastatic lung tumors in mouse models.[16,17] ILC2s could also secrete CXCR2 ligands to reinforce tumor cell-specific apoptosis in solid tumor mouse model,[18] and ILC2s activate

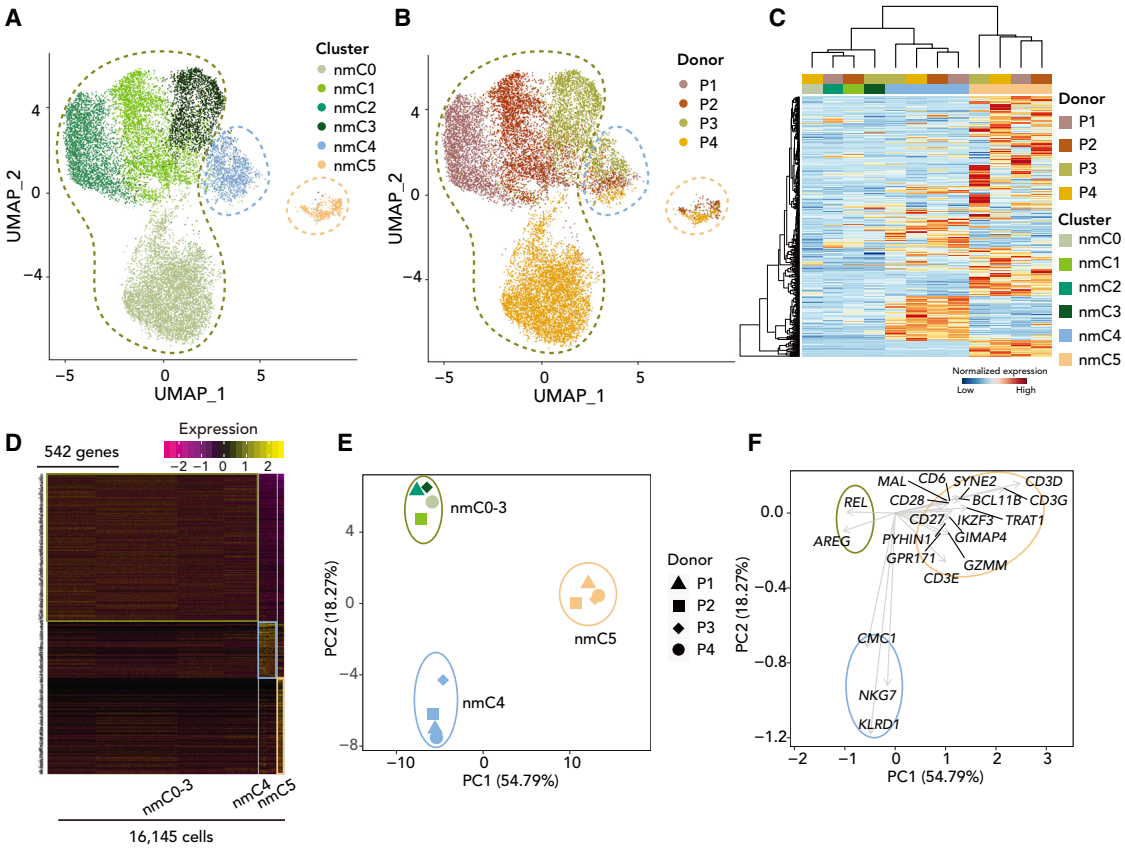

G

	Top 10	Transcription factors	Secreted	Cell membrane
nmC0-3	*CXCL8* *IL4I1* *CD83* *LST1* *IL1R1* *CXCL2* *ATP1B3* *NRIP1* *VEGFA* *NCOA7*	*ZFAND5* *HES1* *ZNF331* *ATF3* *RBPJ* *NR4A3* *ID2* *NFKB1* *NFIL3* *IRF4*	*CXCL8* *IL4I1* *IL1R1* *CXCL2* *VEGFA* *LGALS3* *TNFRSF25* *CSF2* *SDC4* *TNFSF13B*	*CD83* *LST1* *IL1R1* *ATP1B3* *PCDH9* *KIT* *MPV17L* *ICOS* *SCN1B* *TNFRSF25*
nmC4	*GNLY* *KLRD1* *CCL4* *CMC1* *NKG7* *CTSW* *HCST* *EMP3* *CD7* *IFITM2*	*HOPX* *IRF8* *CEBPB* *GATA3* *YBX3* *ZEB2*	*GNLY* *CCL4* *CTSW* *CST7* *XCL2* *LGALS1* *CD55* *GZMK* *NUCB2* *TNFRSF1B*	*KLRD1* *NKG7* *HCST* *EMP3* *CD7* *IFITM2* *CRTAM* *LITAF* *SELL* *FCER1G*
nmC5	*CCL4* *CD3D* *CD3G* *SYNE2* *CCL5* *HSPA1B* *CD3E* *FYB1* *TRAT1* *DNAJB1*	*IKZF3* *BCL11B* *BATF* *ZNF831* *PRDM1* *PBX4* *ID3* *SP140*	*CCL4* *CCL5* *CD40LG* *CST7* *LGALS1* *IFNG* *IL32* *GZMM* *IL6ST* *CD6*	*CD3D* *CD3G* *SYNE2* *CD3E* *TRAT1* *GPR171* *S100A10* *CLEC2D* *CD48* *CD40LG*

H

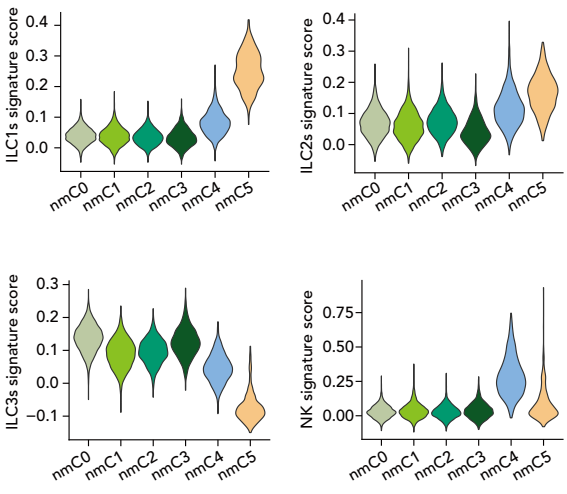

Figure 1. scRNA-seq analysis reveals the presence of ILC1s, ILC3s, and ILC3/NKs, but not ILC2s, in normal mucosa

(A) Uniform manifold approximation and projection (UMAP) plot of 16,145 ILCs from normal mucosa from four patients. Cells are color-coded according to the defined subset.

(B) UMAP with color coding according to donor origin.

(C) Unsupervised hierarchical clustering of the six clusters from each donor on the basis of mean expression levels for genes with variable expression within cells. Samples are color-coded according to their relatedness to a particular subset.

(legend continued on next page)

tissue-specific tumor immunity in pancreatic cancer.[19] ILC3s also have tumor suppressor properties, in the B16 melanoma mouse model[20,21] and in non-small cell lung cancer (NSCLC) patients,[22] for example. In contrast, ILC3-derived IL-17 and IL-22 may contribute to gut cancer development.[23,24] There is, therefore, a clear need to investigate the presence and role of helper-like ILC subsets in various cancer indications.

Colorectal cancer (CRC) is the third most prevalent cancer in both women and men and the second most frequent cause of cancer-related deaths worldwide,[25] despite remarkable improvements in therapeutic strategies. Dysregulated ILC responses have been linked to the development of intestinal cancers. ILC2s are present at low levels in many pathological conditions in humans.[26,27] In contrast, CRC patients have large numbers of ILC1s in the intestines[26–29] and abnormally low levels of ILC3s,[28,29] which normally densely populate the colon at steady state.[27–29] Indeed, decreases in the ILC3/ILC1 ratio have been associated with the severity of CRC.[29] The baseline helper-like ILC landscape, in terms of the composition, diversity, and functional status of these cells in the human gut, remains incompletely explored under tumor conditions.

We used unsupervised hierarchical clustering to investigate helper-like ILC heterogeneity at steady state and during CRC, in the blood, normal mucosa, and gut tumors. The healthy gut is composed of ILC1s, ILC3s, and ILC3/NKs, but no ILC2s. Helper-like ILCs from CRC patients were found to contain two additional subsets: a CRC tissue-specific ILC1-like subset (ctILC1-like) and an ILC2 (ctILC2) subset. SLAMF1 (signaling lymphocytic activation molecule family member 1, CD150) was found to be selectively expressed on ctILCs, and higher frequencies of SLAMF1-expressing helper-like ILCs were found in the blood of CRC patients. The group of patients with SLAMF1-high colon and rectal cancers had a significantly higher survival rate than the SLAMF1-low patients, suggesting that SLAMF1 is an anti-tumor biomarker in CRC.

RESULTS

Healthy gut contains ILC1s, ILC3s, and ILC/NKs, but no ILC2s

We dissected the role of helper-like ILCs in CRC by studying paired CRC tissue and adjacent mucosal tissue (used as a control) samples and comparing blood from patients with blood from age-matched healthy donors (Table S1; Figure S1A). Lineage negative (Lin$^-$) (TCR $\gamma\delta^-$ TCR $\alpha\beta^-$ CD3$^-$ CD19$^-$ CD14$^-$ CD16$^-$ CD94$^-$ CD123$^-$ CD34$^-$ CD303$^-$ FcεRI$^-$) CD127$^+$ helper-like ILCs were more abundant in both normal mucosa and CRC tissue than in blood, consistent with the known tissue residence properties of ILCs[30] (Figures S1B and S1C). The percentage of helper-like ILCs was lower in CRC tissues than in normal mucosa but similar in normal and CRC blood samples (Figures S1B and S1C).

We performed single-cell RNA sequencing (scRNA-seq) on ~58,000 total purified helper-like ILCs from blood samples from CRC patients, healthy blood, normal mucosa, and CRC tissue samples (Figures S1D and S1E). The heterogeneity of helper-like ILCs in normal mucosa was assessed with a total of 16,145 Lin$^-$CD127$^+$ cells from colon tissues adjacent to the colon tumor in CRC patients (Figure S1E). The projection of cells onto two dimensions in a uniform manifold approximation and projection (UMAP) analysis revealed segregation into six distinct clusters: normal mucosa cluster (nmC) 0 to nmC5 (Figure 1A). Two clusters, nmC4 and nmC5, contained cells from all donors, suggesting that there was no donor-specific transcriptomic profile for these two helper-like ILC populations (Figures 1B and 1C). In contrast, most of the cells from nmC0 to nmC3 were single donor specific (Figures 1B and 1C).

Using hierarchical clustering (Figure 1C) and gene signature heatmaps (Figure 1D; Table S2), principal-component analysis (PCA) (Figures 1E and 1F), top ten expressed gene analysis (Figure 1G), and module score analysis (Figure 1H), we then compared the gene signatures of nmC0 to nmC5 with previously described transcriptomic signatures of human helper-like ILC subsets.[31] nmC0 to nmC3 had a common transcriptomic signature characteristic of ILC3s, with *REL*, encoding a proto-oncogene member (c-Rel) of the NF-κB family[32] and NF-κB signaling via the *IL22* promoter site in ILC3s,[33] as a driver gene (Figure 1F), and *KIT*, *CXCL8*, *IL4I1*, and *IL1R1* in the top 10 expressed genes (Figure 1G). nmC4 was characterized by *NKG7*, encoding a cytolytic granule membrane protein,[34] and *KLRD1*, encoding CD94, expressed in T and NK cells, as driver genes, with *GNLY*, *GZMK*, *XCL2*, and *CCL4*, among the top expressed genes and with a whole signature common to NK cells and ILC3s from tonsils (Figures 1F and 1G). nmC4 was thus identified as an ILC3/NK subset. nmC5 resembled ILC1s, with higher levels of expression of T cell markers (*CD3D*, *CD3G*, and *CD3E*), as previously described,[31,35,36] specific transcription factors (*IKZF3*, *BCL 11B*, *PRDM1*, and *ID3*), and NK/ILC1 cell functional cytokines (*GZMM*, *IFNG*, *IL32*, *CCL4*, and *CCL5*) (Figures 1F–1H). nmC0–nmC3 were enriched in response to lipid, glucocorticoid, and corticosteroid, while nmC5 was involved in T cell activation and differentiation (Figure S2A). The assignments of each cluster were supported by the selective expression of known helper-like

(D) Heatmap of the 542 genes (256 in nmC0–nmC3, 97 in nmC4, 189 in nmC5) tested using a Wilcoxon rank-sum test distinguishing the three groups of ILCs in normal mucosa. Cells are plotted in columns, and genes are shown in rows and ranked by adjusted p value < 0.05. Gene expression is color-coded with a scale based on *Z* score distribution from −2.5 (purple) to 2.5 (yellow). Squares identify specific transcriptomic signatures of ILC subsets.
(E) Principal-component analysis (PCA) of the three groups of ILC clusters of each sample on the basis of the mean level of expression for genes with variable expression.
(F) Driving genes for each cell subset, accounting for 20% of the total information in each principal component (PC) from (E).
(G) Top ten expressed genes from the total gene set, and top ten expressed genes encoding transcription factors, secreted proteins, and cell membrane markers significantly differentiating among the groups of ILCs. Gene symbols and annotations were retrieved from public databases. Transcription factor genes are color-coded in red, secreted protein genes in orange, cell membrane protein genes in blue, and other protein-encoding genes in black. Genes encoding both secreted and cell membrane proteins are color-coded in violet. Genes are ranked by p value.
(H) Module score for tonsil ILC gene expression programs for each of the three groups of ILCs, at the single-cell level. Kruskal-Wallis with Dunn's multiple-comparison tests were performed with Benjamini-Hochberg-adjusted p values. Each comparison was statistically significant, and values are shown in Table S3.

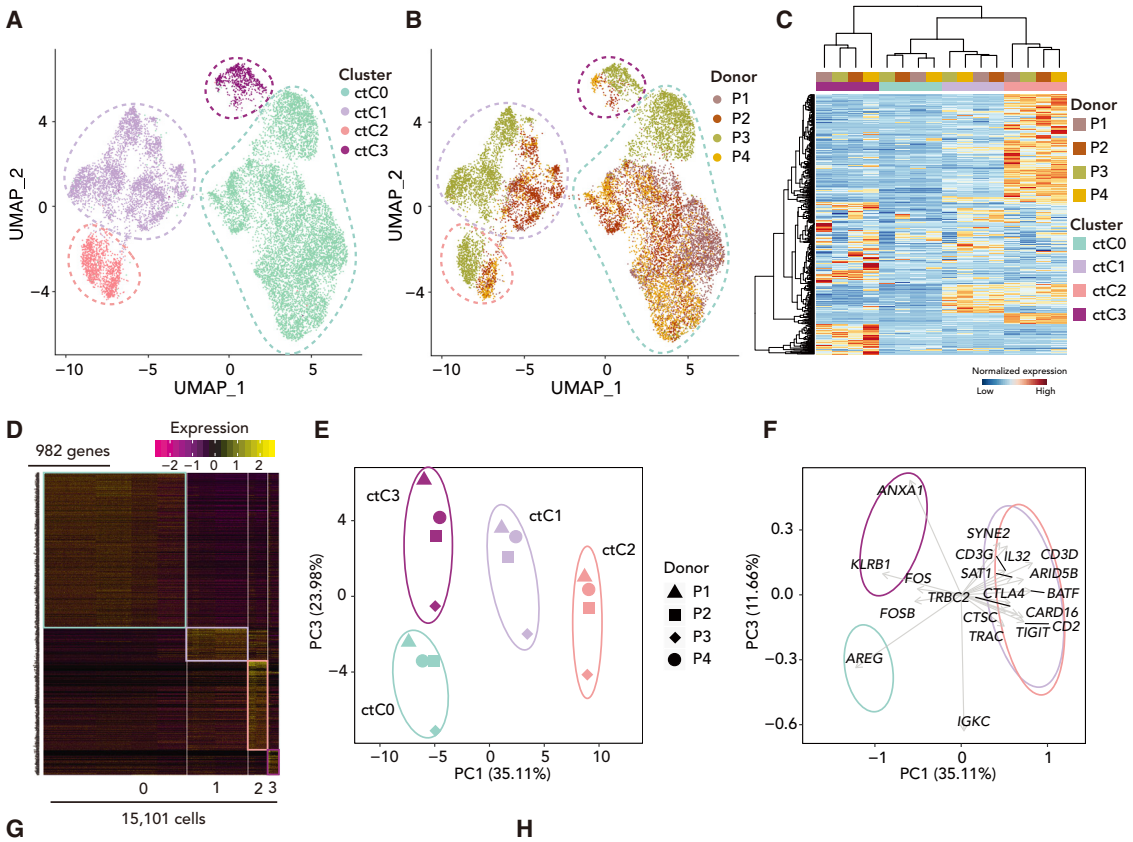

G

	Top 10	Transcription factors	Secreted	Cell membrane
ctC0	*AREG* *KIT* *XCL1* *GNLY* *XCL2* *TYROBP* *NFKB1* *CTSW* *CXCL8* *ZFP36L1*	*NFKB1* *MAFF* *FOSB* *REL* *BHLHE40* *ZNF331* *RBPJ* *NFIL3* *AFF3* *RERE*	*XCL1* *GNLY* *XCL2* *CTSW* *CXCL8* *IL4I1* *VEGFA* *EREG* *TNFSF11* *SPINK2*	*AREG* *KIT* *TYROBP* *LST1* *PCDH9* *FCER1G* *CD81* *SELENOS* *CD83* *EREG*
ctC1	*CCL4* *CCL4L2* *GZMK* *CD3D* *IFNG* *CCL5* *GZMA* *CD3G* *NKG7* *GZMH*	*PRDM1* *ZNF831* *PBX4* *BATF* *IKZF3* *BCL11B* *SP140*	*CCL4* *CCL4L2* *GZMK* *IFNG* *CCL5* *GZMA* *GZMH* *CST7* *ANXA1* *GZMM*	*CD3D* *CD3G* *NKG7* *TRAT1* *SYNE2* *GPR171* *CD3E* *RARRES3* *CD40LG* *CD8A*
ctC2	*BATF* *TIGIT* *CARD16* *SAT1* *CTLA4* *MAGEH1* *CTSC* *LINC01943* *CD27* *ICA1*	*BATF* *FOXP3* *PRDM1* *ZBTB38* *IKZF2* *BLOC1S1* *MAF* *CREM* *ETV7* *PBX4*	*IL32* *LAIR2* *TNFRSF1B* *SLAMF1* *IL1R2* *LGALS1* *ISG15* *NAMPT* *C4orf48* *SPOCK2*	*TIGIT* *CTLA4* *MAGEH1* *CD27* *TNFRSF4* *TNFRSF9* *CLEC2D* *TNFRSF1B* *CD3D* *IL2RA*
ctC3	*IL1RL1* *HPGDS* *SLAMF1* *PLIN2* *IL17RB* *PTGS2* *PMAIP1* *ZFP36L2* *IL2* *HPGD*	*GATA3* *HES4* *RORA* *ZBTB16* *EGR1* *PPARG* *KLF9*	*IL1RL1* *SLAMF1* *IL2* *TNFSF10* *IL32* *DPP4* *FSTL4* *ANXA1*	*IL1RL1* *SLAMF1* *IL17RB* *C1orf162* *CD69* *KLRB1* *PTGER2* *CYSLTR1* *FFAR3* *TNFSF10*

H

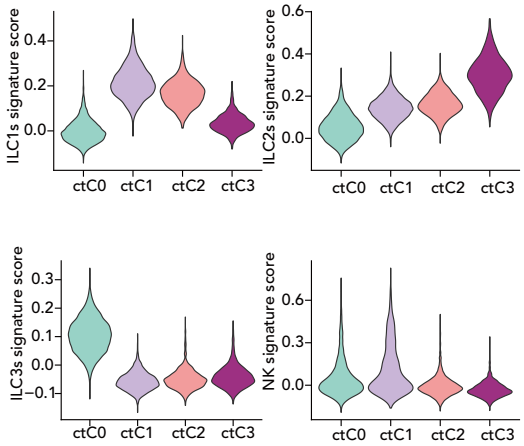

(legend on next page)

ILC markers, such as *IL7R*, *GATA3*, *NCR3*, *EOMES*, *TBX21*, *KIT*, *RORC*, *NCR1*, *NCR2*, and *KLRF1* (Figure S2B). We found differences between nmC5 and previously reported healthy gut ILC1s,[37] probably because the gating strategies used here did not exclude $CD5^+$ cells (Figures S2C and S2D). Thus, the normal gut mucosa defined by scRNA-seq profiling of Lin^-CD127^+ contains ILC1s, ILC3s, and ILCs/NKs, but no ILC2s, consistent with the lack of *PTGDR2* gene expression (Figure S2B).

Tumor ILC1-like and ILC2 subsets are present in CRC patients

We then investigated the composition and diversity of 15,101 ILCs from the tumors of CRC patients. UMAP analysis identified four distinct clusters in CRC tissue: CRC tissue cluster (ctC) 0 to ctC3 (Figure 2A). Contrary to what was observed for normal mucosa, no overwhelming donor-dependent effect was observed, each cluster being present in all samples (Figures 2B and 2C). On the basis of the strategy applied to nmCs (Figure 1), ctC0 was assigned to ILC3s, consistent with its overexpression of *KIT*, *CXCL8*, *NFIL3*, and *IL4I1*, like nmC0–nmC3 (Figures 2C–2H; Table S2). ctC1 resembled ILC1s and, like nmC5, displayed differential expression of genes encoding T cell molecules (*CD3D*, *CD3G*), secreted effectors (*CCL4*, *IFNG*), and ILC-related transcription factors (*IKZF3*, *PRDM1*, and *BCL11B*). The other two subsets present, ctC2 and ctC3, were absent from normal mucosa. ctC2 cells corresponded to an additional ILC1 subset, hereafter called the ctILC1-like subset (CRC tissue-specific ILC1-like subset), characterized by an enrichment in the expression of genes encoding inhibitory and costimulatory markers (*TIGIT*, *CTLA4*, and *TNFRSF4*). ctC3 cells, identified as ILC2s and hereafter referred to as ctILC2, had high levels of expression for genes encoding transcription factors required for ILC2 development (*GATA3*, *RORA*, and *ZBTB16*) and ILC2-responsive cytokine receptor genes (*IL1RL1* and *IL17RB*) (Figures 2C–2H; Table S2). ctC1 was enriched in cytolysis, granulocyte chemotaxis, and granzyme-mediated apoptotic signaling pathway, whereas ctC2 and ctC3 were respectively enriched in T cell anergy and interleukin-5 production and interleukin-13 secretion (Figure S2E). Subset assignments were supported by the selective expression of known ILC markers, such as *IL7R*, *GATA3*, *NCR3*, *EOMES*, *TBX21*, *KIT*, *RORC*, *NCR1*, *NCR2*, and *KLRF1* (Figure S2F). In particular, *PTGDR2* and higher levels of *GATA3* expression were found in the ILC2s. *SLAMF1* (signaling lymphocytic activation molecule family member 1 or CD150), which encodes a soluble and membrane protein involved in the activation of T cells, B cells, and NK cells,[38] was upregulated both in ctILC1-like and ctILC2 in tumors (Figure 2G). Thus, like nmILCs, ctILCs formed heterogeneous populations encompassing four different subsets: ctC0 (resembling ILC3s), ctC1 (resembling ILC1s), ctC2 (named as ILC1-like), and ctC3 (resembling ILC2s).

Tumor tissue ILC3s seemed to be less heterogeneous than those in the normal mucosa. We therefore focused on nmC0–nmC3, nmC4, and ctC0, comparing ILC3 heterogeneity between normal mucosa helper-like ILCs and gut ctILCs, with the same analysis pipeline as described above after applying a correction that removed the donor batch effect, allowing the analysis of ILC3 heterogeneity (Figure S3; Table S2). Four different populations were found in ILC3s from both types of tissue (Figures S3A–S3I), including a potentially immature *SELL*-expressing population, and a population enriched in HLA-encoding transcripts also present in human tonsils (Figures S3E and S3J). Each subset of normal mucosa ILC3 had a counterpart in tumor tissue (Figure S3K). Given the overlap in ILC3s heterogeneity between normal mucosa and gut ctILCs, we can conclude that CRC did not affect the subset heterogeneity of ILC3s. Thus, gut ctILCs differed from nmILCs in the appearance of a ctILC2 subset and a second ctILC1-like subset.

Blood helper-like ILC heterogeneity is stable in CRC

We searched for potential biomarkers of the disease by investigating differences in blood helper-like ILCs between healthy individuals and CRC patients. A UMAP analysis of 19,603 helper-like ILCs from healthy donors revealed three distinct clusters, hereafter referred to as nbC0, nbC1, and nbC2 (Figures S4A–S4C; Table S2). nbC0 was considered to correspond to ILC1s, on the basis of the upregulation of *CD3D*, *CD3E*, *CD3G*, the NK/ILC1 cell effector proteins (*CCL5*, *GZMK*, *GZMM*, and *GZMA*), and helper-like ILC transcription factors (*BCL11B*, *PRDM1*, and *IKZF3*) (Figures S4D–S4H). nbC1 was identified as ILC3s and was characterized by ILC3 transcription factors (*MAFF*, *RUNX3*) and costimulation markers (*TNFRSF4*, *TNFRSF18*). nbC2 displayed an upregulation of genes from the ILC2 signature (*GATA3*, *RORA*) and genes encoding regulatory receptors (*KLRB1*, *KLRG1*) (Figures S4D–S4H). These assignments were supported by the selective expression of known helper-like ILC markers, such as *IL7R*, *GATA3*, *NCR3*, *EOMES*, *TBX21*, *PTGDR2*, *KIT*, *RORC*, *NCR1*, and *KLRF1* (Figure S4I).

Figure 2. scRNA-seq analysis reveals tumor-specific ILC1 and ILC2 subsets in CRC tissues

(A) UMAP plot of 15,101 CRC tissue ILCs (ctILCs) from the CRC tissues of four patients. Cells are color-coded according to the defined subset.

(B) UMAP with color coding for donor origin.

(C) Unsupervised hierarchical clustering of the four clusters from each donor on the basis of mean expression levels for genes with variable expression.

(D) Heatmap of the 982 genes (463 in ctC0, 100 in ctC1, 314 in ctC2, 105 in ctC3) tested using a Wilcoxon rank-sum test distinguishing among the four ctILC subsets in tumor tissue. Cells are plotted in columns, and genes are shown in rows and ranked by adjusted p values (<0.05). Gene expression is color-coded with a scale based on *Z* score distribution from −2.5 (purple) to 2.5 (yellow). Squares identify specific transcriptomic signatures of ctILC subsets.

(E) Principal-component analysis (PCA) of the four ctILC subsets of each sample on the basis of the mean level of expression of genes with variable expression.

(F) Driving genes for each cell subset accounting for 20% of the total information in each PC from (E).

(G) Top ten expressed genes from the total gene set and top ten expressed genes encoding transcription factors, secreted proteins, and cell membrane markers significantly differentiating among the groups of ctILCs. Gene symbols and annotations were retrieved from public databases. Transcription factor genes are color-coded in red, secreted protein genes in orange, cell membrane protein genes in blue, and other protein-encoding genes in black. Genes encoding both secreted and cell membrane proteins are color-coded in violet. Genes are ranked by p value.

(H) Module score for tonsil ILC gene expression programs, at the single-cell level, for each of the four ctILCs subsets. Kruskal-Wallis with Dunn's multiple-comparison tests were performed with Benjamini-Hochberg-adjusted p values. Each comparison was statistically significant, and values are shown in Table S3.

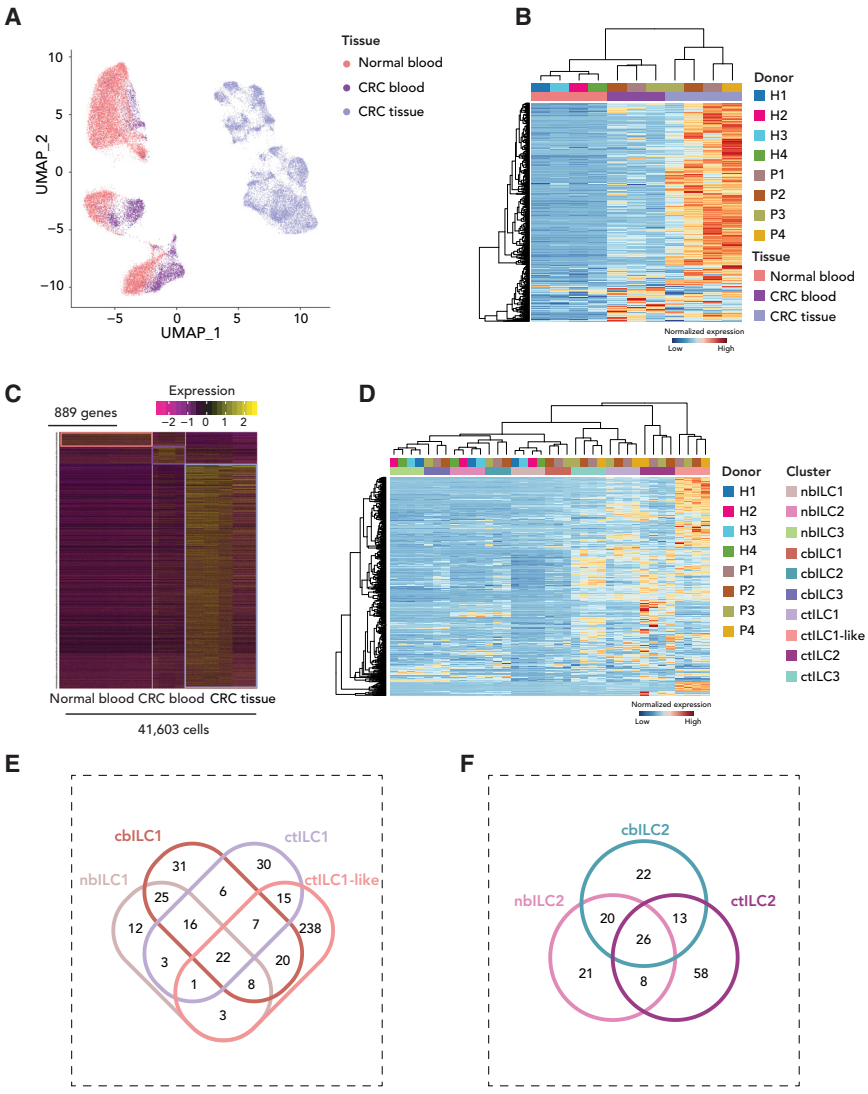

Figure 3. Characterization of tumor tissue-specific ILC subsets

(A) UMAP plot of 41,603 ILCs from normal blood, CRC blood, and CRC tissue. Cells are color-coded according to the defined subset.

(B) Unsupervised hierarchical clustering of normal blood, CRC blood, and CRC tissue ILCs from each donor, on the basis of the mean level of expression of genes with variable expression.

(C) Heatmap of the 889 genes (44 in normal blood, 70 in CRC blood, 775 in CRC tissue) tested in a Wilcoxon rank-sum test distinguishing among the three organs. Cells are plotted in columns, and genes are shown in rows and ranked by adjusted p values (<0.05). Gene expression is color-coded with a scale based on *Z* score distribution from −2.5 (purple) to 2.5 (yellow). Squares identify specific transcriptomic signatures of ILC subsets.

(D) Unsupervised hierarchical clustering of normal blood ILCs (nbILCs), CRC blood ILCs (cbILCs), and CRC tissue ILCs (ctILCs) from each donor, at the subset level, on the basis of the mean expression level for genes with variable expression.

(E) Venn diagram representing the intersection between the gene signatures of the four ILC1 subsets from normal blood, CRC blood, normal mucosa, and CRC tissue.

(F) Venn diagram representing the intersection between the gene signatures of the three ILC2 subsets from normal blood, CRC blood, and CRC tissue.

A UMAP plot of 6,899 blood helper-like ILCs from CRC donors also identified three subsets, hereafter referred to as cbC0, cbC1, and cbC2 (Figures S5A–S5C; Table S2). Driver genes, top ten genes, and module score signatures highlighted the similarity of cbILCs to nbILCs (Figures S5D–S5H). cbC0, like nbC1, had an ILC3 profile with enrichment for *MAFF*, *RUNX3*, and *TNFRSF18*. cbC1 were identified as ILC2s, with high levels of *RORA*, *KLRB1*, *KLRG1*, and *PTGDR2* expression, like nbC2. Of note, similar to ctILC2, cbC1 exhibited high levels of *SLAMF1*. cbC2, like nbC0, displayed enrichment in the genes of the ILC1 signature: *CD3D*, *CD3G*, *CD3E*, *CCL5*, *GZMK*, *GZMM*, *GZMA*, *BCL11B*, *PRDM1*, and *IKZF3* (Figures S5D–S5I). These assignments were also supported by the selective expression of *IL7R*, *GATA3*, *NCR3*, *EOMES*, *TBX21*, *PTGDR2*, *KIT*, *RORC*, *NCR1*, and *KLRF1* (Figure S5I). However, despite the similarity of cbILC subsets to nbILC subsets, velocity analysis predicted a possible conversion of ILC1s into ILC3s only in the context of CRC, in tumor blood (Figure S5J and data not shown). In summary, the blood helper-like ILCs of both healthy donors and CRC patients formed heterogeneous populations containing ILC1, ILC2, and ILC3 subsets.

Identification of a population of CRC tissue-specific ILC1s

Tumor tissue helper-like ILCs contained two additional populations not present in the helper-like ILCs of the normal mucosa, with transcriptomic signatures resembling those of ILC2s and ILC1s (Figures 1 and 2). We investigated the relatedness of these two tumor tissue–specific clusters and the helper-like ILC subsets from healthy blood and blood from CRC patients, by grouping the 41,603 helper-like ILCs into a single global analysis. This analysis revealed organ-specific imprinting in helper-like ILCs, with an overlap between the two types of blood samples, and ctILCs clustering separately (Figure 3A; Table S2). There was a high degree of similarity between nbILCs and cbILCs in gene signature, which was remarkably different from that of ctILCs (Figures 3B and 3C). We further investigated the relationship between defined ILC subsets from CRC tissue, normal blood, and CRC blood samples. The ctILC1-like subset appeared to segregate away from the other clusters, including TILC1 in particular, despite having a core ILC1-transcriptomic signature in common with this subset (Figure 3D). Likewise, another TILC-specific subset, ctILC2, clustered away from the other ctILCs and the ILC2 in the blood. In the blood, each nbILC clustered with the

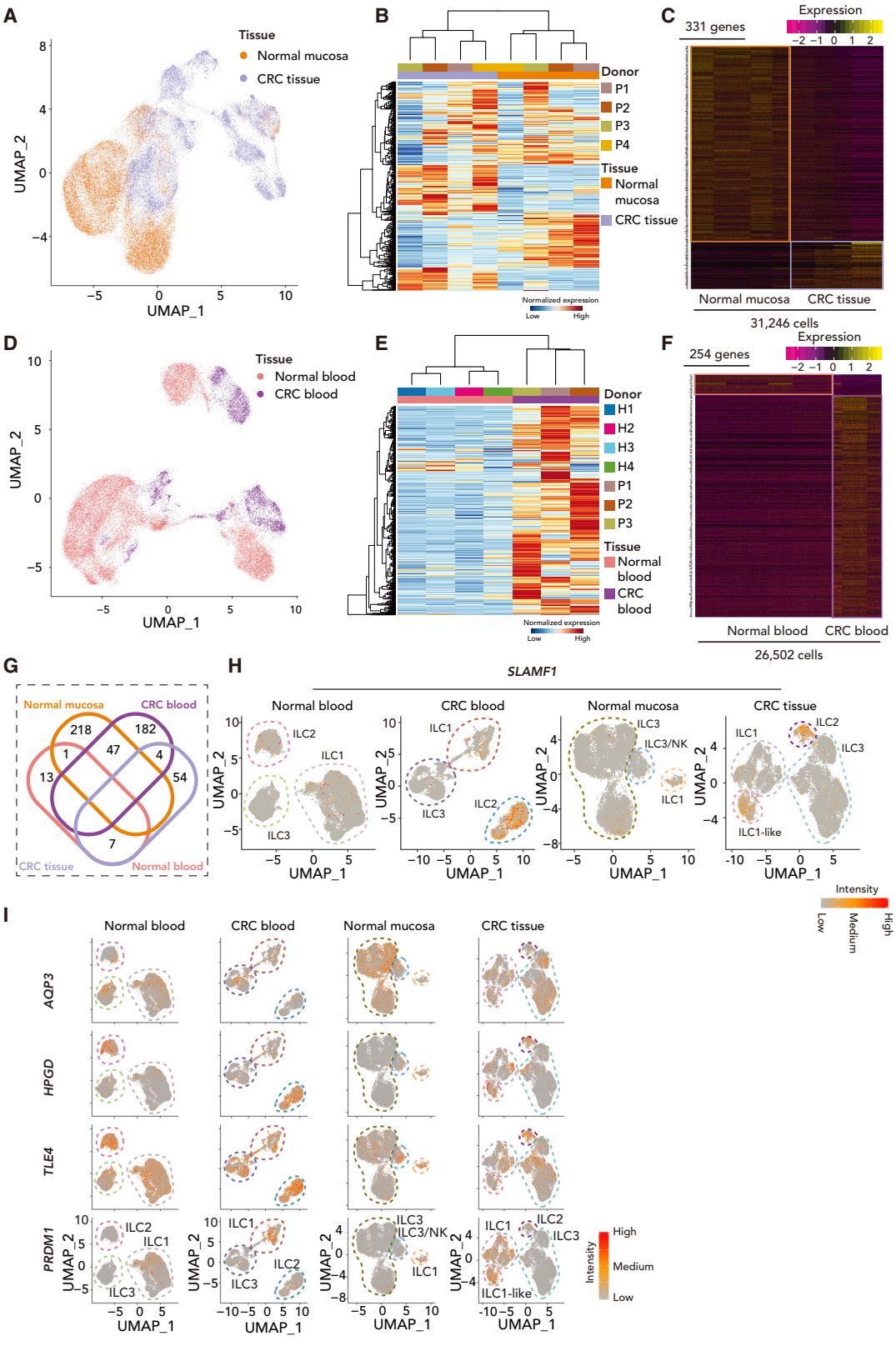

(legend on next page)

corresponding cbILC subset (Figure 3D). We investigated whether the tumor-specific helper-like ILCs shared more genes with their normal blood or CRC blood counterparts by creating Venn diagrams comparing their whole-transcriptomic signatures (Figures 3E and 3F). The ctILC1-like subset shared more genes with cbILC1 (57 genes in common) than with nbILC1 (34 genes in common) (Figure 3E), suggesting tumor imprinting, whereas ctILC2 shared comparable numbers of genes with cbILC2 and nbILC2, with which this subset had 39 and 34 genes, respectively, in common (Figure 3F).

Helper-like ILC signature is modified in CRC tumor

We searched for tumor-specific tissue features of ILCs, by clustering the 31,246 helper-like ILC cells from normal mucosa and tumor tissues. These two tissues had some helper-like ILC populations in common, but UMAP highlighted a shift between the two tissues, suggesting differences at the transcriptomic level (Figure 4A). Unsupervised hierarchical clustering also showed the tissue-of-origin signature to be stronger than the helper-like ILC subset identity signature (Figures 4B and 4C; Table S2). The clustering of nbILCs and cbILCs revealed a similar pattern of separation for the 26,502 helper-like ILCs in the UMAP analysis (Figure 4D) and in unsupervised hierarchical clustering, which segregated blood samples according to health status, revealing differences in transcription between the two subsets (Figures 4E and 4F). One gene was found to be upregulated in normal blood and mucosa (*AQP3*). Four genes were identified as upregulated in both CRC blood and gut ctILCs relative to their healthy counterparts (*SLAMF1*, *HPGD*, *TLE4*, and *PRDM1*) (Figure 4G). Feature plots of these five genes of interest confirmed the specific upregulation of *SLAMF1*, *HPGD*, *TLE4*, and *PRDM1* in gut ctILCs and the downregulation of *AQP3* (Figures 4H and 4I). *SLAMF1* was the principal surface protein gene upregulated in tumors. This gene was expressed in ctILC2, ctILC1-like subsets, and cbILC2 (Figures 2G and 4H; Figure S5) but only weakly in their healthy counterparts (Figure 4H), suggesting that SLAMF1 expression at the helper-like ILC cell surface can differentiate healthy individuals from CRC patients.

SLAMF1 is a biomarker of CRC

We confirmed, using flow cytometry, the expansion of the ILC1 subset accompanied by reduction of the ILC3 subset in tumor tissues from CRC patients relative to adjacent normal mucosa (Figures 5A and 5B). Consistent with the scRNA-seq analysis revealing higher levels of *TIGIT* in an ILC1-like subset and the presence of ctILC2s (Figure 2G), we observed by flow cytometry a population of TIGIT$^+$ ctILC1-like cells and ctILC2 in tumors, but not in normal tissue (Figures 5A and 5B). Higher levels of expression of the ILC2-activating cytokine *IL33* in tumors were correlated with longer survival in CRC patients from The Cancer Genome Atlas (TCGA) dataset, suggesting that ctILC2 might be indicative of a good prognosis in CRC patients (Figure 5C). In contrast to the findings for gut helper-like ILCs, the frequency of each helper-like ILC subset among total helper-like ILCs in blood was similar in CRC patients and healthy donors (Figure 5D). Larger numbers of ILCs expressing SLAMF1 at their surface were found in tumors than in the adjacent tissues, from which SLAMF1 was almost absent (Figures 5E and 5F). In contrast, SLAMF1 was expressed by blood ILCs from healthy donors, but high frequencies of SLAMF1-expressing helper-like ILCs were also found in the blood of CRC patients (Figure 5G). Signatures of *SLAMF1*$^+$ and *SLAMF1*$^-$ ILCs from CRC tissue were then compared. While *RORA* and *IL32* expression were relatively high in *SLAMF1*$^+$ ILCs, *XCL2* and *XCL1* expression were enriched in *SLAMF1*$^-$ ILCs (Figure 5H). IL-32 was reported to be anti-tumor in several cancer types, including cervical, colon, prostate, liver, and pancreatic cancer, as well as melanoma and chronic myeloid leukemia,[39] suggesting that *SLAMF1*$^+$ ILCs might exhibit an *IL-32*-dependent anti-tumor effect. We then investigated the potential role of SLAMF1 in CRC disease development and progression further, by studying the clinical outcome of cancer patients from TCGA database. Survival was much higher in patients with *SLAMF1*-high colon and rectal cancer than in those with *SLAMF1*-low tumors (Figures 5I and 5J), strongly suggesting that SLAMF1 is an anti-tumor biomarker in CRC.

DISCUSSION

Over the past decade, helper-like ILCs have emerged as key elements in protection against pathogens, tissue remodeling, and homeostasis.[8] The contribution of helper-like ILCs to cancer remains poorly understood, as they may promote tumor-associated inflammation or, conversely, may display anti-tumor properties, depending on the tumor microenvironment.

Figure 4. Specific gene signature of ILC in CRC

(A) UMAP plot of 31,246 ILCs from normal mucosa and CRC tissue. Cells are color-coded according to the defined subset.

(B) Unsupervised hierarchical clustering of normal mucosa and CRC tissue ILCs from each donor on the basis of the mean level of expression for genes with variable expression.

(C) Heatmap of the 331 genes (266 in normal mucosa, 65 in CRC tissue) tested using a Wilcoxon rank-sum test distinguishing between the two organs. Cells are plotted in columns, and genes are shown in rows and ranked by adjusted p value (<0.05). Gene expression is color-coded with a scale based on *Z* score distribution from −2.5 (purple) to 2.5 (yellow). Squares identify specific transcriptomic signatures of ILC subsets.

(D) UMAP plot of 26,502 ILCs from normal blood and CRC blood. Cells are color-coded according to the defined subsets.

(E) Unsupervised hierarchical clustering of normal blood and CRC blood ILCs from each donor, on the basis of the mean level of expression of genes with variable expression.

(F) Heatmap of the 254 genes (233 in CRC blood, 21 in normal blood) tested using a Wilcoxon rank-sum test distinguishing between the two organs. Cells are plotted in columns, and genes are shown in rows and ranked by adjusted p value (<0.05). Gene expression is color-coded with a scale based on *Z* score distribution from −2.5 (purple) to 2.5 (yellow). Squares identify specific transcriptomic signatures of ILC subsets.

(G) Venn diagram representing the intersection of gene signatures between normal blood and CRC blood and between normal mucosa and CRC tissue.

(H) Feature plots of relative levels of *SLAMF1* expression on each of the ILCs from normal blood, CRC blood, normal mucosa, and tumor tissue.

(I) Feature plots of the relative expression levels of *AQP3*, *HPGD*, *TLE4*, and *PRDM1* in normal blood, blood from CRC patients, normal mucosa, and tumor tissue.

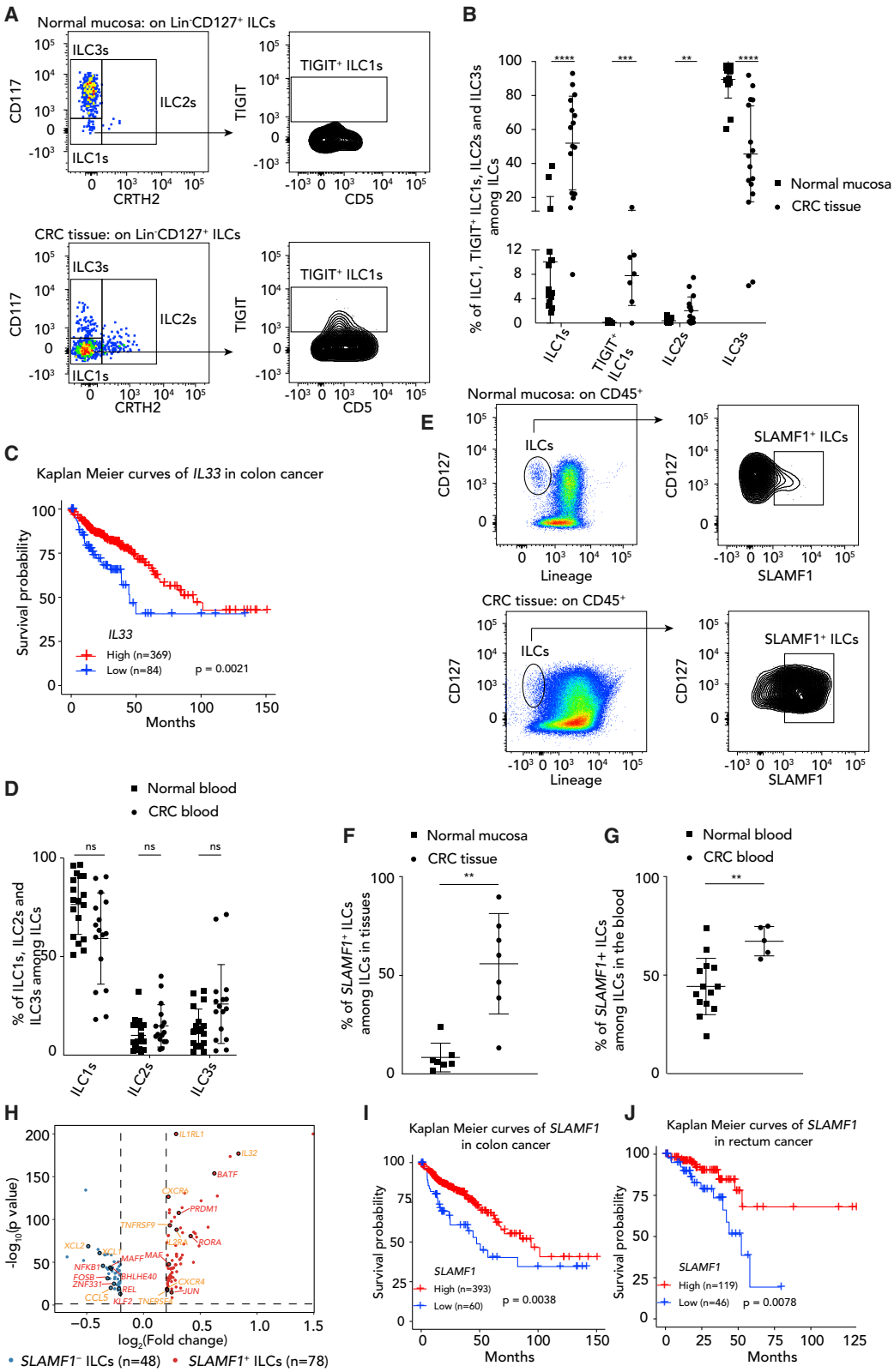

(legend on next page)

We investigated the heterogeneity of helper-like ILCs in the human gut and blood by building a single-cell transcriptomic landscape of Lin$^-$CD127$^+$ cells at steady state and in CRC patients. This unbiased helper-like ILC characterization differed from the analysis of gut ILC transcriptomes provided by another recent study, in which these cells were subjected to sorting by flow cytometry on the basis of the CD103, CD300LF, and CD196 cell surface markers before transcriptomic profiling.[40] We show here by scRNA-seq that the healthy gut contains ILC1s, ILC3s, a population of ILC3/NKs, but no ILC2s. Indeed, only few ILC2s could be detected by flow cytometry as Lin$^-$ CRTH2$^+$ in our analysis and in Trabanelli et al.[41] In a recent study,[37] only 2 of 18 donors exhibited reliable ILC2 populations in colon lamina propria (2.7% and 3.9% of Lin$^-$ CRTH2$^+$), but the vast majority (16 donors) did not possess solid ILC2 subsets (0%–0.6% of Lin$^-$ CRTH2$^+$). Thus, purification of these cells for RNA sequencing was not successfully achieved.[37] Importantly, even if few ILC2s may be present in the intestine of some donors, these cells did not give rise to a robust cluster detectable by scRNA-seq, taking into account the minimal percentage of cells needed to exclude a possible doublet contamination. Indeed, and in contrast to what has been reported for mice, ILC2s are almost entirely absent from healthy human tissues, with the exception of the lungs, adipose tissue, and the blood connective tissue.[41] In our study, we detected tumor-infiltrating ctILC2s in CRC patients. ctILC2s were also observed in breast,[42] gastric,[42] and pancreatic[19] tumors and in urine from bladder cancer patients.[15] Several data support a model in which ILC2s infiltrate tumors via an IL-33-dependent pathway[15,16,19] and mediate tumor immune surveillance by promoting cytolytic CD8$^+$ T cell responses. IL-33 expression showed different survival prognosis in different cancer types, with better prognosis in melanoma patients but not in those with lung squamous cell carcinoma and pancreatic adenocarcinoma.[43] IL-33 is overexpressed in colorectal tumors,[44] and high levels of IL-33 are frequently observed in low-grade adenocarcinomas and early colorectal tumors.[45] Survival rate is higher in the IL-33-high group of colon cancer patients than in IL-33-low patients, suggesting that ctILC2 might be indicative of a good prognosis in CRC. However, PD-1 expression on ctILC2 from late stage of CRC may be of poor prognosis.[46] There is therefore a clear need to investigate further the role of ctILC2s in anti-tumor immunity in CRC and other cancer indications.

We identified an additional helper-like ILC1 subset, called ctILC1-like TIGIT$^+$, present in tumors from CRC patients but absent from the blood. ctILC1-like TIGIT$^+$ had a transcriptional profile more closely resembling the ILC1 gene signature than that of any other ILCs, but they segregated away from ctILC1, suggesting that they differed markedly from "conventional" gut ctILC1. ILC1-like cells known as "intermediate ILC1s" (intILC1s) have also been described in a mouse model of methylcholanthrene (MCA)-induced tumors.[47] In humans, CD56$^+$CD16$^-$ ILC1-like cells have been found in solid tumors and in peritoneal and pleural fluids from cancer patients,[48] and the cytotoxic functions of these cells are altered in the peripheral blood of donors with acute myeloid leukemia.[49] Intratumoral intILC1 may emerge from NK cell differentiation driven by TGF-β signaling, a phenomenon known as ILC plasticity.[47,50] The conversion of ILC3s into ILC1s upon TGF-β signaling has been demonstrated in humanized mice, and a transitional ILC3-ILC1 population has been identified in the human intestine.[40] We observed no such phenomenon in our gut ILC dataset, and none of the algorithms tested was able to establish a relatedness between ctILC1-like TIGIT$^+$ and another gut ILC subset reflecting possible differentiation (data not shown). The mechanisms by which ctILC1-like TIGIT$^+$ emerge in CRC tumors thus remain to be determined. We observed a plasticity of ILC1 toward ILC3 in the blood of CRC patients, but not in healthy donors, suggesting the presence of soluble signals driving ILC1-ILC3 plasticity, such as sustained IL-23 levels.[51] The biological relevance of such ILC1-ILC3 plasticity in the blood of CRC patients is not clear.

intILC1s and ILC1s produced large amounts of TNF-α and were found to be ineffective at controlling carcinogenesis, potentially even promoting metastasis in mouse models.[47] In human, CD56$^+$CD16$^-$ ILC1-like cells express the pro-angiogenic factor VEGF, which may also favor tumor growth.[48] In CRC patients, the frequency of ILC1s has been shown to be higher in tumor tissues than in the normal mucosa[28,29] and to increase, at

Figure 5. SLAMF1 is a biomarker in CRC

(A) Representative flow cytometry profile of TIGIT cell surface expression on the ctILC1-like subset.

(B) Flow cytometry analysis of ILC subsets from normal mucosa (n = 8–16) and CRC tissues (n = 7–16). Data show the frequencies of the indicated subset among total ILCs.

(C) Kaplan-Meier curves of overall survival stratified by IL-33 expression in CRC patients from TCGA. The optimal cut-off for patient stratification was obtained using a Cox proportional hazards model, and the p value was calculated using a log rank test. IL-33-high group, n = 369; IL-33-low group, n = 84.

(D) Flow cytometry analysis of blood ILC subsets from healthy donors (n = 18) and CRC patients (n = 16).

(E) Representative fluorescence-activated cell sorting (FACS) profile of SLAMF1 cell surface expression on ILCs.

(F) Flow cytometry analysis of SLAMF1 expression on total ILCs from normal mucosa (n = 7) and CRC tissues (n = 7). The data show frequencies of SLAMF1$^+$ cells among total ILCs.

(G) Flow cytometry analysis of SLAMF1 expression on total blood ILCs from healthy donors (n = 14) and CRC patients (n = 5). Data show frequencies of SLAMF1$^+$ cells among total ILCs.

(H) Differentially expressed (DE) genes between *SLAMF1*$^+$ ILCs and *SLAMF1*$^-$ ILCs in CRC tissues. The DE transcriptional factors and cytokines are labeled by red and orange text, respectively. Red dots indicate genes upregulated in *SLAMF1*$^+$ ILCs, and blue dots represent genes upregulated in *SLAMF1*$^-$ ILCs.

(I and J) Kaplan-Meier curves for overall survival stratified by SLAMF1 expression level in colon (I) and rectum (J) cancer patients from TCGA. The optimal cut-off for patient stratification was obtained with a Cox proportional hazards model, and the p value was calculated using a log rank test. In (I), *SLAMF1*-high group, n = 393; *SLAMF1*-low group, n = 60. In (J), *SLAMF1*-high group, n = 119; *SLAMF1*-low group, n = 46.

In (B) and (D), statistical significance was calculated using Kruskal-Wallis tests with Dunn's multiple-comparison tests, and p values were adjusted using the Benjamini-Hochberg method. In (F) and (G), Mann-Whitney tests of unpaired nonparametric t tests were used. In (H), statistical analysis was performed using the Wilcoxon test. *p < 0.05, **p < 0.01, ***p < 0.001, and ****p < 0.0001.

the expense of ILC3s, with tumor progression.[29] These results suggest that high ILC1 levels may be predictive of a poor prognosis in cancer. The issue of the specific biological function of the ctILC1-like subset relative to classical TILC1 in CRC tumors also needs to be addressed, because ctILC1-like cells have high levels of PD1 and TIGIT and may be further unleashed by anti-PD1 and anti-TIGIT immunotherapies.

We characterized the levels of three subsets, ILC3, ILC3/NK, and ILC1, in the normal mucosa of all donors. A donor-specific effect was observed in the ILC3 subsets, suggesting possible ILC3 imprinting by the microbiota. This effect was absent in blood ILC3 population from healthy donors, which was similar to CRC patient blood. Thus, alteration of gut microbiota did not seem to influence ILC3 population in the blood. One explanation could reside in the fact that ILC3s are largely resident in tissues.[52] Interestingly, CRC tumors had much lower levels of ILC3s and displayed a loss of this apparent donor specificity. CRC is frequently associated with tumor dysbiosis, involving massive changes to the composition of the microbiota.[53–57] ILC3s are major regulators of intestinal barrier integrity and immune homeostasis. It might therefore be beneficial to promote both ILC3 recolonization and diversification in CRC patients. ILC3 heterogeneity could potentially be boosted by increasing microbial diversity.

We also defined a population of ILC3/NK cells in healthy gut mucosa. These cells had transcriptomic features in common with both ILC3 and NK cells. They differ from ILC3s mostly in terms of their *NKG7*, *KLRD1* (CD94), *GNLY*, *GZMK*, *XCL2*, and *CCL4* expression. The biological role of this ILC3/NK subset and its relatedness to "classical" ILC3 remain to be addressed.

A recent study in a mouse model of CRC confirmed the diversity of ILC populations present within the tumor.[46] The authors identified six subsets of helper ILC encompassing one ILC1, three ILC2 (A, B, and C), one ILC3, and one "ILCreg." That study also presented results obtained using flow cytometry in human colorectal tumors that corroborated the presence of $PD1^+$ ILC2 and ILCreg in patients with advanced CRC. We did not found these populations in our study, which is based on the analysis of donors with early stage disease. However, these results suggest the need for an additional comparative scRNA-seq study to understand the evolution of the heterogeneity of helper-like ILC as the disease progresses.

SLAMF1 was the only cell surface marker for which transcript levels were higher in ctILCs and blood ILCs from CRC patients. ILCs expressing SLAMF1 on their surface were also present at higher frequency in tumors and blood from CRC patients than in healthy donors. SLAMF1 is a single-chain type I transmembrane receptor bearing two immunoreceptor tyrosine-based switch motifs (ITSM) in its cytoplasmic tail, thus recruiting Src homology 2 (SH2) domain-containing signal transduction molecules such as SLAM-associated protein (SAP) to initiate downstream signaling cascades.[38,58,59] SLAMF1 is a self-ligand but also a microbial receptor for morbilliviruses and a bacterial sensor involved in the elimination of Gram-negative bacteria.[38,60–62] SLAMF1 is expressed by almost all hematopoietic cells except NK cells, particularly those with an activated phenotype and is upregulated upon cell activation.[38,63] A large proportion of ILCs in the bloodstream expressed SLAMF1 on their surface at steady state, but no such expression was observed on ILCs from normal gut mucosa. In contrast, SLAMF1 was expressed on ctILCs from CRC patients, suggesting that ctILCs may be more activated in the tumor bed than in the normal adjacent mucosa. Nevertheless, the effect of SLAMF1 engagement at the cell surface of helper-like ILCs on the biology of these cells remains to be investigated. High levels of SLAMF1 were correlated with better survival of CRC patients. Our results therefore suggest that SLAMF1 is an anti-tumor biomarker in CRC.

ILCs have emerged as tissue-specific modulators of cancer immunity that can control various aspects of immunotherapy. As ILCs and T cells co-exist in human cancers and have stimulatory and inhibitory pathways in common, immunotherapy strategies targeting anti-cancer ILCs may be as important as strategies targeting T cells. Our results suggest that ILCs are part of the tumor microenvironment, as subsets of ctILCs are present in CRC. It is tempting to speculate that they may regulate immunity at the tumor bed or have a direct effect on tumor cells. Further studies are required to determine whether it is possible to define more tumor-specific subsets differing in terms of activation status, with either pro- or anti-tumor immunity effects, in cancers arising in different tissues.

Limitations of the study

In this study we mainly used scRNA-seq technology to decipher the heterogeneity of ILCs in healthy donor and CRC patients. We did not found ILC2s in normal mucosa by scRNA-seq but in tumors. The mechanisms involved in the recruitment and differentiation of ILC2s in CRC tumors remain to be investigated. The functions of tumor-specific ILC1-like cells and $SLMAF1^+$ ILCs were not addressed in this first study.

STAR★METHODS

Detailed methods are provided in the online version of this paper and include the following:

- KEY RESOURCES TABLE
- RESOURCE AVAILABILITY
  - Lead contact
  - Materials availability
  - Data and code availability
- EXPERIMENTAL MODEL AND SUBJECT DETAILS
- METHOD DETAILS
  - Isolation of human cells from intestine and blood samples
  - Sorting of ILCs
  - Flow cytometry for ILCs
  - Single-cell RNA sequencing
  - Raw 10X read alignment, quality control and normalization
  - Filtering contaminated cells
  - Reduction of the number of dimensions and clustering
  - Batch effect correction for ILC3 subsets in normal and tumor mucosa
  - Unsupervised hierarchical clustering
  - Principal component analysis
  - Differential expression analysis

- Gene annotations
- RNA velocity estimation
- Scoring samples for ILC signatures
- TCGA analysis

- QUANTIFICATION AND STATISTICAL ANALYSIS

SUPPLEMENTAL INFORMATION

Supplemental information can be found online at https://doi.org/10.1016/j.xcrm.2021.100353.

ACKNOWLEDGMENTS

This work was supported by grants from the National Natural Science Foundation of China (31930035, 91942311, and 81971487) and the Shanghai Science and Technology Commission (20JC1410100).

AUTHOR CONTRIBUTIONS

Conceptualization, J.Q., A.C., E.V., and B.S.; Investigation, J.Q. and A.C.; Formal Analysis, J.Q., A.C., B.E., Y.Y., and L.B.; Validation, J.Q.; Resources, Z.W., T.Z., L.H., Y.L., H.L., N.W., M.Z., and L.C.; Writing – Original Draft, J.Q., A.C., L.S., Y.Y., B.S., E.N.-M., and E.V.; Writing – Review & Editing, J.Q., A.C., L.S., B.S., E.N.-M., and E.V.; Funding Acquisition, L.S. and B.S.; Supervision, L.S., E.N.-M., E.V., and B.S.

DECLARATION OF INTERESTS

E.V. is an Innate Pharma employee. Patents related to this work were under application.

Received: December 22, 2020
Revised: March 29, 2021
Accepted: June 24, 2021
Published: July 27, 2021

REFERENCES

1. Baumeister, S.H., Freeman, G.J., Dranoff, G., and Sharpe, A.H. (2016). Co-inhibitory pathways in immunotherapy for cancer. Annu. Rev. Immunol. *34*, 539–573.
2. Chen, D.S., and Mellman, I. (2017). Elements of cancer immunity and the cancer-immune set point. Nature *541*, 321–330.
3. Okazaki, T., Chikuma, S., Iwai, Y., Fagarasan, S., and Honjo, T. (2013). A rheostat for immune responses: the unique properties of PD-1 and their advantages for clinical application. Nat. Immunol. *14*, 1212–1218.
4. Schumacher, T.N., and Schreiber, R.D. (2015). Neoantigens in cancer immunotherapy. Science *348*, 69–74.
5. Sharma, P., and Allison, J.P. (2015). Immune checkpoint targeting in cancer therapy: toward combination strategies with curative potential. Cell *161*, 205–214.
6. Okazaki, T., and Honjo, T. (2007). PD-1 and PD-1 ligands: from discovery to clinical application. Int. Immunol. *19*, 813–824.
7. Spits, H., Artis, D., Colonna, M., Diefenbach, A., Di Santo, J.P., Eberl, G., Koyasu, S., Locksley, R.M., McKenzie, A.N., Mebius, R.E., et al. (2013). Innate lymphoid cells—a proposal for uniform nomenclature. Nat. Rev. Immunol. *13*, 145–149.
8. Vivier, E., Artis, D., Colonna, M., Diefenbach, A., Di Santo, J.P., Eberl, G., Koyasu, S., Locksley, R.M., McKenzie, A.N.J., Mebius, R.E., et al. (2018). Innate lymphoid cells: 10 years on. Cell *174*, 1054–1066.
9. López-Soto, A., Gonzalez, S., Smyth, M.J., and Galluzzi, L. (2017). Control of metastasis by NK cells. Cancer Cell *32*, 135–154.
10. Chiossone, L., Dumas, P.Y., Vienne, M., and Vivier, E. (2018). Natural killer cells and other innate lymphoid cells in cancer. Nat. Rev. Immunol. *18*, 671–688.
11. Castro, F., Cardoso, A.P., Gonçalves, R.M., Serre, K., and Oliveira, M.J. (2018). Interferon-gamma at the crossroads of tumor immune surveillance or evasion. Front. Immunol. *9*, 847.
12. Zaidi, M.R. (2019). The interferon-gamma paradox in cancer. J. Interferon Cytokine Res. *39*, 30–38.
13. Bie, Q., Zhang, P., Su, Z., Zheng, D., Ying, X., Wu, Y., Yang, H., Chen, D., Wang, S., and Xu, H. (2014). Polarization of ILC2s in peripheral blood might contribute to immunosuppressive microenvironment in patients with gastric cancer. J. Immunol. Res. *2014*, 923135.
14. Trabanelli, S., Chevalier, M.F., Martinez-Usatorre, A., Gomez-Cadena, A., Salomé, B., Lecciso, M., Salvestrini, V., Verdeil, G., Racle, J., Papayannidis, C., et al. (2017). Tumour-derived PGD2 and NKp30-B7H6 engagement drives an immunosuppressive ILC2-MDSC axis. Nat. Commun. *8*, 593.
15. Chevalier, M.F., Trabanelli, S., Racle, J., Salomé, B., Cesson, V., Gharbi, D., Bohner, P., Domingos-Pereira, S., Dartiguenave, F., Fritschi, A.S., et al. (2017). ILC2-modulated T cell-to-MDSC balance is associated with bladder cancer recurrence. J. Clin. Invest. *127*, 2916–2929.
16. Saranchova, I., Han, J., Huang, H., Fenninger, F., Choi, K.B., Munro, L., Pfeifer, C., Welch, I., Wyatt, A.W., Fazli, L., et al. (2016). Discovery of a metastatic immune escape mechanism initiated by the loss of expression of the tumour biomarker interleukin-33. Sci. Rep. *6*, 30555.
17. Ikutani, M., Yanagibashi, T., Ogasawara, M., Tsuneyama, K., Yamamoto, S., Hattori, Y., Kouro, T., Itakura, A., Nagai, Y., Takaki, S., and Takatsu, K. (2012). Identification of innate IL-5-producing cells and their role in lung eosinophil regulation and antitumor immunity. J. Immunol. *188*, 703–713.
18. Kim, J., Kim, W., Moon, U.J., Kim, H.J., Choi, H.J., Sin, J.I., Park, N.H., Cho, H.R., and Kwon, B. (2016). Intratumorally establishing type 2 innate lymphoid cells blocks tumor growth. J. Immunol. *196*, 2410–2423.
19. Moral, J.A., Leung, J., Rojas, L.A., Ruan, J., Zhao, J., Sethna, Z., Ramnarain, A., Gasmi, B., Gururajan, M., Redmond, D., et al. (2020). ILC2s amplify PD-1 blockade by activating tissue-specific cancer immunity. Nature *579*, 130–135.
20. Eisenring, M., vom Berg, J., Kristiansen, G., Saller, E., and Becher, B. (2010). IL-12 initiates tumor rejection via lymphoid tissue-inducer cells bearing the natural cytotoxicity receptor NKp46. Nat. Immunol. *11*, 1030–1038.
21. Nussbaum, K., Burkhard, S.H., Ohs, I., Mair, F., Klose, C.S.N., Arnold, S.J., Diefenbach, A., Tugues, S., and Becher, B. (2017). Tissue microenvironment dictates the fate and tumor-suppressive function of type 3 ILCs. J. Exp. Med. *214*, 2331–2347.
22. Carrega, P., Loiacono, F., Di Carlo, E., Scaramuccia, A., Mora, M., Conte, R., Benelli, R., Spaggiari, G.M., Cantoni, C., Campana, S., et al. (2015). NCR(+)ILC3 concentrate in human lung cancer and associate with intratumoral lymphoid structures. Nat. Commun. *6*, 8280.
23. Chan, I.H., Jain, R., Tessmer, M.S., Gorman, D., Mangadu, R., Sathe, M., Vives, F., Moon, C., Penaflor, E., Turner, S., et al. (2014). Interleukin-23 is sufficient to induce rapid de novo gut tumorigenesis, independent of carcinogens, through activation of innate lymphoid cells. Mucosal Immunol. *7*, 842–856.
24. Kirchberger, S., Royston, D.J., Boulard, O., Thornton, E., Franchini, F., Szabady, R.L., Harrison, O., and Powrie, F. (2013). Innate lymphoid cells sustain colon cancer through production of interleukin-22 in a mouse model. J. Exp. Med. *210*, 917–931.
25. Bray, F., Ferlay, J., Soerjomataram, I., Siegel, R.L., Torre, L.A., and Jemal, A. (2018). Global cancer statistics 2018: GLOBOCAN estimates of incidence and mortality worldwide for 36 cancers in 185 countries. CA Cancer J. Clin. *68*, 394–424.
26. Fuchs, A., Vermi, W., Lee, J.S., Lonardi, S., Gilfillan, S., Newberry, R.D., Cella, M., and Colonna, M. (2013). Intraepithelial type 1 innate lymphoid

cells are a unique subset of IL-12- and IL-15-responsive IFN-γ-producing cells. Immunity *38*, 769–781.

27. Simoni, Y., Fehlings, M., Kløverpris, H.N., McGovern, N., Koo, S.L., Loh, C.Y., Lim, S., Kurioka, A., Fergusson, J.R., Tang, C.L., et al. (2017). Human innate lymphoid cell subsets possess tissue-type based heterogeneity in phenotype and frequency. Immunity *46*, 148–161.
28. Carrega, P., Orecchia, P., Quatrini, L., Tumino, N., Venè, R., Benelli, R., Poggi, A., Scabini, S., Mingari, M.C., Moretta, L., and Vacca, P. (2020). Characterisation of innate lymphoid cell subsets infiltrating colorectal carcinoma. Gut *69*, 2261–2263.
29. Ikeda, A., Ogino, T., Kayama, H., Okuzaki, D., Nishimura, J., Fujino, S., Miyoshi, N., Takahashi, H., Uemura, M., Matsuda, C., et al. (2020). Human NKp44+ group 3 innate lymphoid cells associate with tumor-associated tertiary lymphoid structures in colorectal cancer. Cancer Immunol. Res. *8*, 724–731.
30. Gasteiger, G., Fan, X., Dikiy, S., Lee, S.Y., and Rudensky, A.Y. (2015). Tissue residency of innate lymphoid cells in lymphoid and nonlymphoid organs. Science *350*, 981–985.
31. Björklund, A.K., Forkel, M., Picelli, S., Konya, V., Theorell, J., Friberg, D., Sandberg, R., and Mjösberg, J. (2016). The heterogeneity of human CD127(+) innate lymphoid cells revealed by single-cell RNA sequencing. Nat. Immunol. *17*, 451–460.
32. Grinberg-Bleyer, Y., Oh, H., Desrichard, A., Bhatt, D.M., Caron, R., Chan, T.A., Schmid, R.M., Klein, U., Hayden, M.S., and Ghosh, S. (2017). NF-κB c-Rel is crucial for the regulatory T cell immune checkpoint in cancer. Cell *170*, 1096–1108.e13.
33. Victor, A.R., Nalin, A.P., Dong, W., McClory, S., Wei, M., Mao, C., Kladney, R.D., Youssef, Y., Chan, W.K., Briercheck, E.L., et al. (2017). IL-18 drives ILC3 proliferation and promotes IL-22 production via NF-κB. J. Immunol. *199*, 2333–2342.
34. Medley, Q.G., Kedersha, N., O'Brien, S., Tian, Q., Schlossman, S.F., Streuli, M., and Anderson, P. (1996). Characterization of GMP-17, a granule membrane protein that moves to the plasma membrane of natural killer cells following target cell recognition. Proc. Natl. Acad. Sci. U S A *93*, 685–689.
35. Ercolano, G., Wyss, T., Salomé, B., Romero, P., Trabanelli, S., and Jandus, C. (2020). Distinct and shared gene expression for human innate versus adaptive helper lymphoid cells. J. Leukoc. Biol. *108*, 723–737.
36. Robinette, M.L., Fuchs, A., Cortez, V.S., Lee, J.S., Wang, Y., Durum, S.K., Gilfillan, S., and Colonna, M.; Immunological Genome Consortium (2015). Transcriptional programs define molecular characteristics of innate lymphoid cell classes and subsets. Nat. Immunol. *16*, 306–317.
37. Yudanin, N.A., Schmitz, F., Flamar, A.L., Thome, J.J.C., Tait Wojno, E., Moeller, J.B., Schirmer, M., Latorre, I.J., Xavier, R.J., Farber, D.L., et al. (2019). Spatial and temporal mapping of human innate lymphoid cells reveals elements of tissue specificity. Immunity *50*, 505–519.e4.
38. Gordiienko, I., Shlapatska, L., Kovalevska, L., and Sidorenko, S.P. (2019). SLAMF1/CD150 in hematologic malignancies: silent marker or active player? Clin. Immunol. *204*, 14–22.
39. Hong, J.T., Son, D.J., Lee, C.K., Yoon, D.Y., Lee, D.H., and Park, M.H. (2017). Interleukin 32, inflammation and cancer. Pharmacol. Ther. *174*, 127–137.
40. Cella, M., Gamini, R., Sécca, C., Collins, P.L., Zhao, S., Peng, V., Robinette, M.L., Schettini, J., Zaitsev, K., Gordon, W., et al. (2019). Subsets of ILC3-ILC1-like cells generate a diversity spectrum of innate lymphoid cells in human mucosal tissues. Nat. Immunol. *20*, 980–991.
41. Trabanelli, S., Gomez-Cadena, A., Salomé, B., Michaud, K., Mavilio, D., Landis, B.N., Jandus, P., and Jandus, C. (2018). Human innate lymphoid cells (ILCs): toward a uniform immune-phenotyping. Cytometry B Clin. Cytom. *94*, 392–399.
42. Salimi, M., Wang, R., Yao, X., Li, X., Wang, X., Hu, Y., Chang, X., Fan, P., Dong, T., and Ogg, G. (2018). Activated innate lymphoid cell populations accumulate in human tumour tissues. BMC Cancer *18*, 341.
43. Wagner, M., Ealey, K.N., Tetsu, H., Kiniwa, T., Motomura, Y., Moro, K., and Koyasu, S. (2020). Tumor-derived lactic acid contributes to the paucity of intratumoral ILC2s. Cell Rep. *30*, 2743–2757.e5.
44. Cui, G., Qi, H., Gundersen, M.D., Yang, H., Christiansen, I., Sørbye, S.W., Goll, R., and Florholmen, J. (2015). Dynamics of the IL-33/ST2 network in the progression of human colorectal adenoma to sporadic colorectal cancer. Cancer Immunol. Immunother. *64*, 181–190.
45. Mertz, K.D., Mager, L.F., Wasmer, M.H., Thiesler, T., Koelzer, V.H., Ruzzante, G., Joller, S., Murdoch, J.R., Brümmendorf, T., Genitsch, V., et al. (2015). The IL-33/ST2 pathway contributes to intestinal tumorigenesis in humans and mice. OncoImmunology *5*, e1062966.
46. Wang, S., Qu, Y., Xia, P., Chen, Y., Zhu, X., Zhang, J., Wang, G., Tian, Y., Ying, J., and Fan, Z. (2020). Transdifferentiation of tumor infiltrating innate lymphoid cells during progression of colorectal cancer. Cell Res. *30*, 610–622.
47. Gao, Y., Souza-Fonseca-Guimaraes, F., Bald, T., Ng, S.S., Young, A., Ngiow, S.F., Rautela, J., Straube, J., Waddell, N., Blake, S.J., et al. (2017). Tumor immunoevasion by the conversion of effector NK cells into type 1 innate lymphoid cells. Nat. Immunol. *18*, 1004–1015.
48. Levi, I., Amsalem, H., Nissan, A., Darash-Yahana, M., Peretz, T., Mandelboim, O., and Rachmilewitz, J. (2015). Characterization of tumor infiltrating natural killer cell subset. Oncotarget *6*, 13835–13843.
49. Salomé, B., Gomez-Cadena, A., Loyon, R., Suffiotti, M., Salvestrini, V., Wyss, T., Vanoni, G., Ruan, D.F., Rossi, M., Tozzo, A., et al. (2019). CD56 as a marker of an ILC1-like population with NK cell properties that is functionally impaired in AML. Blood Adv. *3*, 3674–3687.
50. Cortez, V.S., Cervantes-Barragan, L., Robinette, M.L., Bando, J.K., Wang, Y., Geiger, T.L., Gilfillan, S., Fuchs, A., Vivier, E., Sun, J.C., et al. (2016). Transforming growth factor-β signaling guides the differentiation of innate lymphoid cells in salivary glands. Immunity *44*, 1127–1139.
51. Koh, J., Kim, H.Y., Lee, Y., Park, I.K., Kang, C.H., Kim, Y.T., Kim, J.E., Choi, M., Lee, W.W., Jeon, Y.K., and Chung, D.H. (2019). IL23-producing human lung cancer cells promote tumor growth via conversion of innate lymphoid cell 1 (ILC1) into ILC3. Clin. Cancer Res. *25*, 4026–4037.
52. Dutton, E.E., Gajdasik, D.W., Willis, C., Fiancette, R., Bishop, E.L., Camelo, A., Sleeman, M.A., Coccia, M., Didierlaurent, A.M., Tomura, M., et al. (2019). Peripheral lymph nodes contain migratory and resident innate lymphoid cell populations. Sci. Immunol. *4*, eaau8082.
53. Feng, Q., Liang, S., Jia, H., Stadlmayr, A., Tang, L., Lan, Z., Zhang, D., Xia, H., Xu, X., Jie, Z., et al. (2015). Gut microbiome development along the colorectal adenoma-carcinoma sequence. Nat. Commun. *6*, 6528.
54. Liang, Q., Chiu, J., Chen, Y., Huang, Y., Higashimori, A., Fang, J., Brim, H., Ashktorab, H., Ng, S.C., Ng, S.S.M., et al. (2017). Fecal bacteria act as novel biomarkers for noninvasive diagnosis of colorectal cancer. Clin. Cancer Res. *23*, 2061–2070.
55. Nakatsu, G., Li, X., Zhou, H., Sheng, J., Wong, S.H., Wu, W.K., Ng, S.C., Tsoi, H., Dong, Y., Zhang, N., et al. (2015). Gut mucosal microbiome across stages of colorectal carcinogenesis. Nat. Commun. *6*, 8727.
56. Yazici, C., Wolf, P.G., Kim, H., Cross, T.L., Vermillion, K., Carroll, T., Augustus, G.J., Mutlu, E., Tussing-Humphreys, L., Braunschweig, C., et al. (2017). Race-dependent association of sulfidogenic bacteria with colorectal cancer. Gut *66*, 1983–1994.
57. Yu, J., Feng, Q., Wong, S.H., Zhang, D., Liang, Q.Y., Qin, Y., Tang, L., Zhao, H., Stenvang, J., Li, Y., et al. (2017). Metagenomic analysis of faecal microbiome as a tool towards targeted non-invasive biomarkers for colorectal cancer. Gut *66*, 70–78.
58. Vilar, M.L., Frutuoso, M.S., Arruda, S.M., Lima, D.M., Bezerra, C.S., and Pompeu, M.M. (2011). The role of the SLAM-SAP signaling pathway in the modulation of CD4+ T cell responses. Braz. J. Med. Biol. Res. *44*, 276–282.
59. Romero, X., Sintes, J., and Engel, P. (2014). Role of SLAM family receptors and specific adapter SAP in innate-like lymphocytes. Crit. Rev. Immunol. *34*, 263–299.

60. Yurchenko, M., Skjesol, A., Ryan, L., Richard, G.M., Kandasamy, R.K., Wang, N., Terhorst, C., Husebye, H., and Espevik, T. (2018). SLAMF1 is required for TLR4-mediated TRAM-TRIF-dependent signaling in human macrophages. J. Cell Biol. *217*, 1411–1429.

61. Berger, S.B., Romero, X., Ma, C., Wang, G., Faubion, W.A., Liao, G., Compeer, E., Keszei, M., Rameh, L., Wang, N., et al. (2010). SLAM is a microbial sensor that regulates bacterial phagosome functions in macrophages. Nat. Immunol. *11*, 920–927.

62. Song, T., Dong, C., and Xiong, S. (2015). Signaling lymphocyte-activation molecule SLAMF1 augments mycobacteria BCG-induced inflammatory response and facilitates bacterial clearance. Int. J. Med. Microbiol. *305*, 572–580.

63. Romero, X., Benítez, D., March, S., Vilella, R., Miralpeix, M., and Engel, P. (2004). Differential expression of SAP and EAT-2-binding leukocyte cell-surface molecules CD84, CD150 (SLAM), CD229 (Ly9) and CD244 (2B4). Tissue Antigens *64*, 132–144.

64. Butler, A., Hoffman, P., Smibert, P., Papalexi, E., and Satija, R. (2018). Integrating single-cell transcriptomic data across different conditions, technologies, and species. Nat. Biotechnol. *36*, 411–420.

65. Falcon, S., and Gentleman, R. (2007). Using GOstats to test gene lists for GO term association. Bioinformatics *23*, 257–258.

66. Aran, D., Looney, A.P., Liu, L., Wu, E., Fong, V., Hsu, A., Chak, S., Naikawadi, R.P., Wolters, P.J., Abate, A.R., et al. (2019). Reference-based analysis of lung single-cell sequencing reveals a transitional profibrotic macrophage. Nat. Immunol. *20*, 163–172.

67. Stuart, T., Butler, A., Hoffman, P., Hafemeister, C., Papalexi, E., Mauck, W.M., 3rd, Hao, Y., Stoeckius, M., Smibert, P., and Satija, R. (2019). Comprehensive integration of single-cell data. Cell *177*, 1888–1902.e21.

68. Khan, A., Fornes, O., Stigliani, A., Gheorghe, M., Castro-Mondragon, J.A., van der Lee, R., Bessy, A., Chèneby, J., Kulkarni, S.R., Tan, G., et al. (2018). JASPAR 2018: update of the open-access database of transcription factor binding profiles and its web framework. Nucleic Acids Res. *46* (*D1*), D260–D266.

69. Wilson, D., Charoensawan, V., Kummerfeld, S.K., and Teichmann, S.A. (2008). DBD—taxonomically broad transcription factor predictions: new content and functionality. Nucleic Acids Res. *36*, D88–D92.

70. Hu, H., Miao, Y.R., Jia, L.H., Yu, Q.Y., Zhang, Q., and Guo, A.Y. (2019). AnimalTFDB 3.0: a comprehensive resource for annotation and prediction of animal transcription factors. Nucleic Acids Res. *47* (*D1*), D33–D38.

71. Pujato, M., Kieken, F., Skiles, A.A., Tapinos, N., and Fiser, A. (2014). Prediction of DNA binding motifs from 3D models of transcription factors; identifying TLX3 regulated genes. Nucleic Acids Res. *42*, 13500–13512.

72. Uhlén, M., Fagerberg, L., Hallström, B.M., Lindskog, C., Oksvold, P., Mardinoglu, A., Sivertsson, Å., Kampf, C., Sjöstedt, E., Asplund, A., et al. (2015). Proteomics. Tissue-based map of the human proteome. Science *347*, 1260419.

73. La Manno, G., Soldatov, R., Zeisel, A., Braun, E., Hochgerner, H., Petukhov, V., Lidschreiber, K., Kastriti, M.E., Lönnerberg, P., Furlan, A., et al. (2018). RNA velocity of single cells. Nature *560*, 494–498.

STAR★METHODS

KEY RESOURCES TABLE

REAGENT or RESOURCE	SOURCE	IDENTIFIER
Antibodies		
Fc Receptor Blocking Solution	BioLegend	Cat#422302; RRID:AB_2818986
Anti-human TCR gd antibody, clone B1, FITC	BD Biosciences	Cat# 559878; RRID:AB_397353
Anti-human TCR ab antibody, clone T10B9.1A-31, FITC	BD Biosciences	Cat# 555547; RRID:AB_395931
Anti-human CD3 antibody, clone UCHT1, FITC	BD Biosciences	Cat# 555916; RRID:AB_396217
Anti-human CD19 antibody, clone HIB19, FITC	BD Biosciences	Cat# 555412; RRID:AB_395812
Anti-human CD14 antibody, clone M5E2, FITC	BD Biosciences	Cat# 555397; RRID:AB_395798
Anti-human CD16 antibody, clone 3G8, FITC	BD Biosciences	Cat# 555406; RRID:AB_395806
Anti-human CD94 antibody, clone HP-3D9, FITC	BD Biosciences	Cat# 555888; RRID:AB_396200
Anti-human CD123 antibody, clone 7G3, FITC	BD Biosciences	Cat# 558663; RRID:AB_1645485
Anti-human CD34 antibody, clone 581, FITC	BD Biosciences	Cat# 555821; RRID:AB_396150
Anti-human CD303 (BDCA-2) antibody, clone AC144, FITC	Miltenyi Biotec	Cat# 130-090-510; RRID:AB_244167
Anti-human FceR1 alpha antibody, clone (AER-37 (CRA1)), FITC	Thermo Fisher Scientific	Cat# 11-5899-42; RRID:AB_10732835
Anti-human CD127 antibody, clone eBioRDR5, PE	Thermo Fisher Scientific	Cat# 12-1278-42; RRID:AB_10717663
Anti-human CD45 antibody, clone 2D, Alexa Fluor 700	Thermo Fisher Scientific	Cat# 56-9459-42; RRID:AB_2574511
Anti-human CD117 (c-kit) antibody, clone 104D2, BV421	BioLegend	Cat# 313216; RRID:AB_11148721
Anti-human CD294 (CRTH2) antibody, clone BM16, PE-CF594	BD Biosciences	Cat# 563501; RRID:AB_2738244
Anti-human CD45 antibody, clone 2D1, APC-Cy7	BD Biosciences	Cat# 557833; RRID:AB_396891
Anti-human CD117 antibody, clone YB5.B8, PE-Cy5	BD Biosciences	Cat# 559879; RRID:AB_397354
anti-human CD5 antibody, clone UCHT2, Alexa Fluor 700	BD Biosciences	Cat# 561159; RRID:AB_10563911
Anti-human TIGIT (VSTM3) antibody, clone A15153G, PE-Cy7	BioLegend	Cat# 372714, RRID:AB_2632929
Anti-Human CD150 antibody, clone A12, BV421	BD Biosciences	Cat# 562875; RRID:AB_2737858
Chemicals, peptides, and recombinant proteins		
Collagenase Type VIII	Sigma-Aldrich	Cat#C2139
DNase I	Sigma-Aldrich	Cat#DN25
DL-Dithiothreitol	Sigma-Aldrich	Cat#D9779
Lymphoprep	STEMCELL	Cat#07851
Fetal bovine serum	Thermo Fisher Scientific	Cat#10437028
Penicillin-Streptomycin	GIBCO	Cat#5140122
RPMI 1640	Corning	Cat#10-041-CV
Phosphate Buffered Saline	Corning	Cat#21-040-CMR
Fixable Viability Stain 520	BD Horizon	Cat#564407
Fixable Viability Stain 620	BD Horizon	Cat#564996
Normal Mouse Serum	Jackson ImmunoResearch Laboratories	Cat#015-000-120
Brilliant Stain Buffer	BD Horizon	Cat#563794
EDTA	Invitrogen	Cat#AM9260G

(*Continued on next page*)

Continued

REAGENT or RESOURCE	SOURCE	IDENTIFIER
Critical commercial assays		
Chromium Single Cell 3′ Reagent Kits	10X Genomics	Cat#1000121
Deposited data		
scRNA-seq data	This paper	GSA-Human (HRA000919)
Software and algorithms		
Cell Ranger Version 2.2	10x Genomics	https://support.10xgenomics.com/single-cell-gene-expression/software/pipelines/latest/what-is-cell-ranger
Seurat Version 3.2.2	Butler et al.[64]	http://satijalab.org/seurat
R	R Development Core Team, 2008	https://www.r-project.org/
R Studio	N/A	https://www.rstudio.com/
FlowJo Version 10	Tree Star	https://www.flowjo.com/ ; RRID: SCR_008520
GraphPad Prism Version 6	Graphpad	https://www.graphpad.com/ ; RRID: SCR_002798
Gostats Version 2.52.0	Falcon et al.[65]	https://www.bioconductor.org/packages/release/bioc/html/GOstats.html
FastQC Version 0.11.9	Babraham Institue	https://www.bioinformatics.babraham.ac.uk/projects/fastqc/
bcl2fastq2 Conversion Software Version 2.20	Illumina	https://support.illumina.com/downloads/bcl2fastq-conversion-software-v2-20.html
SingleR	Aran et al.[66]	https://github.com/dviraran/SingleR

RESOURCE AVAILABILITY

Lead contact

Further information and resource requests should be directed to and will be fulfilled by the lead contact, Bing Su (bingsu@sjtu.edu.cn).

Materials availability

This study did not generate new materials.

Data and code availability

Raw sequence data of each sample is available to download at Genome Sequence Archive for Human, GSA-Human: HRA000919.

EXPERIMENTAL MODEL AND SUBJECT DETAILS

Clinical samples were obtained from colorectal cancer (CRC) patients without chemo-radiation therapy before resection of the tumor and healthy individuals who gave informed consent, after approval had been obtained from the local medical ethics committee of Ruijin Hospital and Xinhua Hospital Affiliated to Shanghai Jiao Tong University School of Medicine. Four CRC patients were recruited for scRNaseq at diagnosis (Table S1). Adjacent tissue (normal mucosa), and CRC tissue were collected from these four CRC donors whereas blood samples were collected except P4. Healthy blood for scRNaseq were recruited from individuals undergoing routine colonoscopy who were generally in good health, with no other relevant medical history, such as inflammatory bowel disease (IBD) or CRC (Table S1).

METHOD DETAILS

Isolation of human cells from intestine and blood samples

Fresh intestine tissues were quickly placed into 50 mL tubes containing RPMI 1640 medium plus 10% FBS, and were transported on ice to laboratory for cell preparation usually within 2 hours. Adipose tissue and visible blood vessels were removed from the tissue manually. Specimens were weighed and washed with PBS and then cut into small pieces. Normal tissue was incubated with 10 mL freshly prepared intraepithelial lymphocyte solution (5 mM EDTA, 15 mM HEPES, 10% FBS, 1 mM DTT in PBS), for 1 hour at 37°C, with shaking at 200 rpm. CRC tissue was washed with 10 mL freshly prepared 6.5 mM DTT in PBS for 15 min at 37°C, with shaking. After incubation, the tissue pieces were rinsed twice with PBS and subjected to enzymatic digestion for 1 hour at 37°C, with shaking

(0.38 mg/mL collagenase VIII, 0.1 mg/mL DNase I, 100 U/ml penicillin, 100 mg/mL streptomycin, 10% FBS in RPMI 1640 medium). The digested tissues were then shaken vigorously by hand for 5 min and mechanically dissociated with a 21-gauge syringe. The resulting cell suspension was filtered through a cell strainer with 100 μm pores into a new 50 mL conical tube, and PBS was added to a final volume of 30 mL. Cells were then centrifuged at 1,800 rpm for 5 min. The supernatants were discarded and the cell pellets were resuspended in RMPI 1640 medium supplemented with 10% FBS. Cells were centrifuged on a Ficoll gradient and then washed with PBS before use.

Peripheral blood mononuclear cells (PBMCs) were obtained from human blood samples centrifuged on a Ficoll gradient. Briefly, blood was mixed with an equal volume of 2% FBS in PBS and gently layered on the Ficoll gradient. Cells were centrifuged at 1000 x *g* for 25 min, without braking. The cells in the middle layer were then washed once with PBS and resuspended in 2% FBS in PBS for use.

Sorting of ILCs

Freshly prepared human cells were resuspended in PBS and incubated with a live/dead cell marker, Fixable Viability stain 520 (BD 564407), for 10 min at 4°C. Cells were washed and suspended in 2% FBS, 2 mM EDTA in PBS (FACS buffer), supplemented with 10% mouse serum and 40% Brilliant Strain Buffer. Cells were first stained with 1:50 human Fc Block for 10 min at 4°C and then incubated with antibodies directed against CD45, CD127, CD117, CRTH2, and against lineage markers (TCRγδ, TCR αβ, CD3, CD19, CD14, CD16, CD94, CD123, CD34, CD303 and FcεRI) for 30 min at room temperature. Human cells were washed with FACS buffer, centrifuged and resuspended in FACS buffer. Live ILCs in RPMI 1640 supplemented with 20% FBS were sorted in a BD FACSAria III cell sorter (BD Biosciences).

Flow cytometry for ILCs

For cell surface staining of ILCs, freshly prepared human cells were stained with live/dead cell markers, Fixable Viability stain 520 (BD 564407), and Fc Block as for ILCs sorting. Cells were stained with surface antibodies against CD45, CD127, CD117, CRTH2, CD5, TIGIT and SLAMF1 and antibodies against same lineage markers for ILCs sorting for 30 min at room temperature. For each of the staining, paired samples from same patients were used. PBMC from more healthy donors was stained at same time. Cells were kept at 4°C and analyzed on a BD Symphony (BD Biosciences). Flow data was analyzed with FlowJo software (FlowJo LLC). Statistical analysis was performed by Mann-Whitney tests of unpaired nonparametric t tests or Kruskal-Wallis tests with Dunn's multiple comparison tests. *p-value*s were adjusted with the Benjamini-Hochberg method for multiple comparison tests. * p-value < 0.05, ** p-value < 0.01, *** p-value < 0.001, **** p-value < 0.0001.

Single-cell RNA sequencing

Purified ILCs were resuspended in PBS supplemented with 0.04% BSA, and kept on ice. Cells were counted and cell density was adjusted to that recommended for 10x Genomics Chromium single-cell 3′ v3 processing and library preparation. Sequencing was performed on an Illumina platform (NovaSeq 6000), by GENERGY BIO (Shanghai, China), at a sequencing depth of about 90,000 reads per single cell.

Raw 10X read alignment, quality control and normalization

Raw sequencing reads were subjected to quality control with FastQC software v0.11.9 (https://www.bioinformatics.babraham.ac.uk/projects/fastqc/). Sequencing data in a bcl file were converted to FASTQ format with Illumina bcl2fastq2 Conversion Software v2.20 (https://support.illumina.com/downloads/bcl2fastq-conversion-software-v2-20.html). We then used Cell Ranger Single Cell Software Suite v. 2.2 to process, align, and summarize unique molecular identifier (UMI) counts, according to the standard pipeline and default parameters described at https://support.10xgenomics.com/single-cell-gene-expression/software/pipelines/latest/what-is-cell-ranger. Briefly, we used the standard Cell Ranger Count pipeline to align FASTQ reads with the GRch38 genome. We then filtered sequencing reads on the basis of base-calling quality scores, and assigned cell barcodes and UMIs to each read. The Cell Ranger aggr pipeline was used to normalize all scRNaseq data with default parameters, to obtain a uniform sequencing depth. The combined feature-barcode matrix was used for downstream analysis.

During quality control with Seurat analysis, raw UMI count matrices were filtered to remove genes expressed in fewer than three cells, cells with fewer than 200 genes, cells with more than 4000 genes, and cells with high percentages of mitochondrial genes (more than 8%). The resulting matrix was then normalized by a global-scaling method, converted with a scaling factor (10,000 by default) and log-transformed with the "LogNormalize" function in Seurat for downstream analysis.

Filtering contaminated cells

We used the R package SingleR[66] and default parameters to assign individual cells to cell types, with the Human Primary Cell Atlas Data as the reference dataset. Each single cell was annotated with a cell type in "label.main" of the dataset. As the dataset did not include the human ILC dataset, and, given the similarities between ILCs and T cells or NK cells, we retained cells labeled as both NK and T cells. We removed cells considered as doublets with an range from 0.14% to 3.69%. In addition, when analyzing the ILC3 in tumor tissue, two small clusters with percentage ranging from 0.35% to 3.59% that were not present in each donor were removed. Donor-specific clusters with a strong specific NK cell signature were considered to be true NK cell contaminants and were removed from downstream analysis.

Reduction of the number of dimensions and clustering

The top 2000 variable genes were selected with the "FindVariableGenes" function of Seurat[67] and used for principal component analysis (PCA). For ILCs in normal mucosa, we retained the first 40 PCs. For normal blood, CRC blood and tumor tissue, we retained the top 20 PCs. Clusters were identified with the "FindClusters" function, with the algorithm based on the optimization of nearest-neighbor modularity implemented in Seurat and visualized with the uniform manifold approximation and projection (UMAP) algorithm. For comparisons of different tissues, the "merge" function was used to pool the individual Seurat objects. For donor and tissue data visualization, the "group.by" parameters were set as intended information when plotting with "DimPlot" function in Seurat.

Batch effect correction for ILC3 subsets in normal and tumor mucosa

ILC3 clusters in tumor tissue and both ILC3 and ILC3/NK clusters in normal mucosa were subsampled for downstream clustering. The batch effect was corrected with the "IntegrateData" function of the standard workflow of Seurat, based on previously identified anchors (Butler et al., 2018[64]).

Unsupervised hierarchical clustering

Mean gene expression was analyzed for single cells in each cluster. Only genes previously shown to display variable expression were used. We used the Heatmap.plus package to plot the unsupervised clustering map. The Euclidean distance was calculated for genes in all clusters. For normal mucosa, only the major donor-derived ILCs for cluster 0-4 were used for analysis.

Principal component analysis

Principal component analysis (PCA) was performed on the mean level of expression of variable genes in clusters. The top 20 genes contributing to PC1 and PC2 or PC1 and PC3 were plotted. For the analysis of ILCs in normal mucosa, we removed ILCs from donors other than the major source of cluster 0-4. PCA gene loadings for the PCs corresponded to the 20 genes making the largest contribution to the total amount of information represented by PC1 and PC2 or PC1 and PC3.

Differential expression analysis

We used the "FindAllMarkers" function in Seurat to identify genes differentially expressed between samples, for each cluster. The non-parametric Wilcoxon rank-sum test was used to obtain p values for comparisons, and the adjusted *p-value*s, based on Bonferroni correction, for all genes in the dataset. We used the following parameters for the calculation of log fold-change (logFC) in expression values and to obtain *p-value*s for all the variable genes for each cluster: min.pct = 0.05, min.diff.pct = 0.1, logfc.threshold = 0.25. The log-transformed and scaled expression values of the genes were used to generate a heatmap.

Gene annotations

Genes encoding transcription factors (TFs) were retrieved from four TF-related public datasets: JASPAR[68] (http://jaspar.genereg.net/), DBD[69], AnimalTFDB[70] (http://bioinfo.life.hust.edu.cn/AnimalTFDB/), and TF2DNA[71] (http://www.fiserlab.org/tf2dna_db/). Genes encoding cell membrane and secreted proteins were obtained from The Human Protein Atlas[72] (https://www.proteinatlas.org/humanproteome/tissue/secretome). Genes were ranked by the adjusted *p-value* for each ILCs cluster in tissue. The top 10 genes within each category (TF, cell membrane, or secreted protein) was selected based on their original adjusted *p-value* in each cluster.

RNA velocity estimation

We analyzed expression dynamics, using scRNA-seq data, by estimating the RNA velocities of single cells by distinguishing between unspliced and spliced transcripts on the basis of the previously aligned bam files of scRNA-seq data. The RNA velocity values for each gene in each cell and the embedding of RNA velocity vectors in a low-dimension space were calculated with the R package velocyto.R[73] (https://github.com/velocyto-team/velocyto.R). RNA velocities were then visualized on the UMAP projection by Gaussian smoothing on a regular grid.

Scoring samples for ILC signatures

ILC and NK cell signatures from tonsil tissue were defined by Björklund et al.,[31]. ILC1 and ILC3 signatures from jejunum, and ILC2 signatures from spleen were obtained from Yudanin et al.,[37]. Module scores were calculated with "AddModuleScore" in Seurat, for each ILC. Briefly, the mean level of gene expression in a single cell was calculated, and the aggregate expression of control feature sets was then subtracted from it. The control features were selected at random from all features. For the module scores of ILC3 subsets from normal mucosa, the differentially expressed gene signatures for each ILC3 subset were used, at single-cell level, on each ILC3 subset in CRC tissues. Violin plots were used to visualize the module scores of each cluster.

TCGA analysis

RNaseq data from primary tumors and clinical annotations were downloaded using the package TCGAbiolinks in September 2019. Kaplan-Meier curves were plotted using the R package survminer. In order to split the expression levels in two groups, the cut-off which gave the lowest p value was used. Optimal cut-off for patient stratification was obtained with a Cox proportional hazards model and p value indicated in the plot was calculated with a log-Rank test.

QUANTIFICATION AND STATISTICAL ANALYSIS

Data are presented as the mean ± standard error of the means (SEM), or standard deviations (SD). GraphPad Prism 6 was used for statistical analysis, two-sided Wilcoxon test and Mann–Whitney test were used for unpaired data. Kruskal-Wallis tests with Dunn's multiple comparison tests was used for multiple comparisons. Kaplan–Meier survival data were analyzed using two-sided log-rank test. p values < 0.05 were considered significantly statistical difference.